Title
The Regulation and Mechanism of Lymphocyte Egress

Author
Shiow, Lawrence Raymond

Publication Date
2008-06-16

Peer reviewed|Thesis/dissertation

The Regulation and Mechanism of Lymphocyte Egress

by

Lawrence R. Shiow

DISSERTATION

Submitted in partial satisfaction of the requirements for the degree of

DOCTOR OF PHILOSOPHY

in

Biomedical Sciences

in the

GRADUATE DIVISION

of the

UNIVERSITY OF CALIFORNIA, SAN FRANCISCO

To my wife, Stephanie.

ACKNOWLEDGEMENTS

This thesis could not have been possible without the many wonderful individuals who I've been fortunate to work with during my graduate training.

I could not have asked for a better graduate mentor than Jason. Despite my poor immunology background, he was willing to take me in as a student, which has been an invaluable experience. As a teacher, Jason has been more than generous with his time and imparting his logic and perspective. Through many patient discussions, his passion for science and teaching showed. By example, Jason has also demonstrated a mature approach to science with regard to handling unexpected setbacks and focusing on the next challenge ahead.

I am also grateful for the mentorship from my thesis committee members Arthur Weiss and Mark Anderson. They always made time for me and welcomed me when I dropped by their offices for discussions. In addition to helpful scientific advice, they have also provided their valuable career perspective as physician-scientists.

I have also been extremely fortunate that my studies have allowed me to work with and learn from two additional physician-scientists: Mehrdad Matloubian and Jennifer Puck. For our CD69 story, I worked at the bench with Mehrdad and learned a great deal from him. For a young graduate student like me, such a close interaction with an experienced scientist was very helpful. I can only hope I didn't bother him too much. For our Coronin-1A project, I benefited from many illuminating discussions with

Jennifer. As an MSTP student, the clinical exposure has been extremely exciting and Jennifer has been an invaluable physician-scientist role model.

It was also great to have Dave Rosen in Lewis Lanier's lab next door. Dave was an excellent source for advice on biochemistry and Starbucks giftcards. I'm also grateful to Lewis for providing the neighborhood with the espresso machine, which has fueled many experiments. And despite her best efforts to the contrary, it has been a fun time working with Susan Watson.

My graduate training would not have been possible without generous funding support from a Genentech Graduate Student Fellowship and the MSTP. Our MSTP directors Arthur Weiss and Kevin Shannon have been great program leaders, but I also owe big thanks to Jana Toutolmin and Catherine Norton at the MSTP office and Lisa Magargal at the BMS office for making everything run so smoothly.

The lab has been a fantastic environment and I'd like to thank the many past and present Cyster Lab members. I was very fortunate to join a great group of graduate students in the lab. When I first started in the lab, Charles Lo always offered to helped me inject mice and showed me how to do protocols in a time efficient manner. He also organized many fun lab events that centered on eating food. My baymate Robin Lesley always challenged me to consider different interpretations for my results, and I quickly learned that I couldn't sneak sloppy data past her. We also shared a guilty fondness for cheesy music and reality television gossip. From when I started in the lab and until he graduated, Chris Allen was always a reliable source of information, especially on the equipment in the lab. I appreciated his thorough approach to experiments and learned a

great deal of flow cytometry from him. My graduate experience has also been greatly enriched by fellow students who joined the lab after me. Trung Pham and I share interests in egress studies and our MD/PhD training. Trung is also one of the funniest and most generous individuals I know, especially with his fabulous and gourmet cooking. Lisa Kelly also shares our appreciation of great food and I've enjoyed our discussions on interesting NY Times articles that Lisa finds. Before Jesse Green joined the lab, my first opportunity to "mentor" another student was during his rotation. Jesse was a very quick learner and I enjoyed working with him, but I still found the experience quite humbling. It really made me appreciate the challenge of simultaneously thinking about different projects, which Jason seems to accomplish effortlessly.

Jason's lab also has a great group of postdocs with whom I've enjoyed working. I've learned a great deal from Guy Cinamon, who sat next to me for most of my time in the lab. Guy was particularly good at motivating me to throw things away from my bench, pay him money, and take swimming lessons. Susan Schwab also worked on egress and I enjoyed many discussions with her. She helped me through many early experiments before starting her own lab, and I really appreciated her critical and careful approach. Taka Okada always had "cool" movies and I learned many new techniques from him both in and outside the lab (golfing). It's always fun and interesting to discuss science and psychology with Joao Pereira, who brings a lot of passion to his work. It was a lot of fun to hang out and snowboard with him and Trung at Keystone (in addition to attending talks). Irina Grigorova also went to the Keystone meeting with us, and showed us her Russian ice skating skills. Her mathematics and microscopy skills have been a

great help to this thesis project. I've also enjoyed Irina's efforts to liven up the bay with Russian jokes. After Guy returned to Israel, Tri Phan moved into his spot and has been a great baymate. I've benefited from many delicious meals that he brings in for lunch. I've also really enjoyed our discussions on science and medicine, and how we can try to form a career between both worlds.

I've been very fortunate to work with Ying Xu, our lab's talented molecular biologist. I've enjoyed her pictures from travels and home as well as her delicious cheesecakes and other baked goods. Jinping An has also been an important help for the thesis work and I've enjoyed many of Jinping's scrumptious dumplings. Olivia Lam also helped out with mouse husbandry, and I'm awe of her talented artwork. Joan Junkin, our lab mom, brought a special spirit to the lab, and I'll always remember the special birthday party she threw for Jason.

My family has been a great source of support during my graduate training. My parents May and Sam have always encouraged me to work hard in pursuing my interests. My sister Lois and her husband Doug have also been wonderfully supportive and have offered helpful advice. And I've been warmly welcomed into my wife's family, especially by her kind and caring parents Linda and Eric.

And last, but certainly not least, I'd like to thank my wife Stephanie. Throughout the years, she has been there to share in my happiness and to brighten up my frustrations. This thesis is dedicated to her because I couldn't have accomplished my graduate studies without her constant love and support.

THE REGULATION AND MECHANISM OF LYMPHOCYTE EGRESS

Lawrence R. Shiow

ABSTRACT

Lymphocyte and thymocyte egress are poorly understood processes that are required for proper immune function. In the periphery, naïve lymphocytes must egress from secondary lymphoid organs to recirculate and travel to other tissues. From the thymus, mature thymocytes must egress to populate the T cell compartment that surveys the periphery. The G-protein coupled receptor (GPCR) sphingosine-1-phosphate receptor-1 ($S1P_1$) is intrinsically required for both egress steps, but how $S1P_1$ promotes egress remains unclear.

First, we studied the role of the early activation antigen CD69 during lymph node "shutdown," a transient block in lymphocyte egress triggered by various innate immune stimuli, including type I interferons (IFN-α/β). We found that CD69 interacts with and negatively regulates $S1P_1$, acting downstream of IFN-α/β to promote lymphocyte retention in lymphoid organs. Our study is the first to describe a trafficking function for CD69 and to report an interaction between a C-type lectin and a GPCR.

Next, we studied a spontaneous thymic egress mutant strain carrying the recessive *ptcd* (peripheral T cell deficiency) locus. We found that *ptcd* mice have an intrinsic T cell migration and trafficking defect, and carry a point mutation in the actin regulator Coronin-1A. This mutation causes protein mislocalization and enhanced Arp2/3 inhibition. Our findings contributed new insight to the mechanism of Arp2/3 regulation by Coronin-1A during T cell trafficking, and also prompted us to identify an atypical human T-B+NK+ SCID patient with Coronin-1A deficiency.

Together, these studies contribute to our understanding of the regulation and mechanism of lymphocyte egress. Furthermore, we've provided a mechanism for the lymph node shutdown phenomenon, discovered a novel lectin-GPCR interaction, provided new insight into actin biology, and reported a novel genetic defect in a patient with T-B+NK+ severe combined immunodeficiency.

TABLE OF CONTENTS

LIST OF FIGURES AND TABLES

CHAPTER ONE

CHAPTER TWO

CHAPTER THREE

LIST OF ABBREVIATIONS

APC	Antigen presenting cell
B6	Black-6
CCL21	Chemokine (C-C motif) ligand 21
CTS	Cataract Shionogi
CXCL12	Chemokine (C-X-C motif) ligand 12
CXCL13	Chemokine (C-X-C motif) ligand 13
DNA	Deoxyribonucleic acid
DP	Double positive
EBV	Epstein Barr virus
ENU	N-ethyl-N-nitrosourea
FACS	Fluorescence-Activated Cell Sorter
GPCR	G-protein coupled receptor
GFP	Green fluorescent protein
ICAM	Intercellular adhesion molecule
IFN	Interferon
IFNAR1	Type 1 IFN receptor chain 1
IL	Interleukin
IP3	Inositol triphosphate

koy	Koyaanisqatsi
LCMV	Lymphocytic choriomeningitis virus
LPS	Lipopolysaccharide
mAb	Monoclonal antibody
MHC	Major histocompatibility
mRNA	Messenger ribonucleic acid
MZ	Marginal zone
NK	Natural killer
PCR	Polymerase chain reaction
PLC	Phospholipase C
poly(I:C)	Polyriboinosinic:polyribocytidylic acid
ptcd	Peripheral T cell deficiency
SCID	Severe combined immunodeficiency
S1P	Sphingosine-1-phosphate
$S1P_1$	Sphingosine-1-phosphate receptor type I
SNP	Single nucleotide polymorphism
SP	Single positive
TCR	T cell receptor
TLR	Toll-like receptor

CONTRIBUTIONS TO PRESENTED WORK

The work presented in Chapter 2 "CD69 acts downstream of interferon-α/β to inhibit $S1P_1$ and lymphocyte egress from lymphoid organs" represents a collaborative effort between the Cyster, Matloubian, and Lanier labs. Mehrdad Matloubian, as a postdoctoral fellow in Jason Cyster's lab and as an independent investigator, characterized the poly(I:C) induced shutdown, demonstrated the lymphocyte-intrinsic requirement for IFNAR1, and demonstrated the retention of S1P responsiveness in these cells. This portion of the work encompasses the bulk of Figure 1. Together with Mehrdad, I conducted trafficking and transwell migration experiments with IFNAR1-deficient and CD69-deficient mice with poly(I:C) and LCMV. This portion of the work encompasses the remainder of Figure 1 and the bulk of Figure 2. I explored the interaction between CD69 and $S1P_1$ in WEHI-231 cell lines, which is presented in Figure 3. David B. Rosen, as a graduate student in Lewis Lanier's lab, cloned the CD69-CD3ζ fusion protein, and demonstrated its ability to activate GFP in 2B4 reporter cells. David and I used this reporter assay to demonstrate an interaction between CD69-CD3ζ and $S1P_1$, and conducted pulldowns between CD69 and $S1P_1$ in the WEHI-231 cell line. This portion of the work is in Figure 4a and 4b. Nadezda Brdickova conducted pulldowns between CD69 and $S1P_1$ in the Jurkat cell line, shown in Figure 4c. Ying Xu conducted important RNA isolation and QPCR reactions. Ying Xu and Jinping An assisted with cloning constructs used in assays for Figures 3 and 4. Olivia Lam assisted with mouse husbandry.

The work presented in Chapter 3 "Coronin-1A is mutated in a thymic egress defective mutant and a T-B+NK+ SCID patient" represents a collaborative effort between the Cyster, Puck, Bear, and Goodnow labs. I conducted the migration and trafficking assays of *ptcd* mice that encompass the bulk of Figure 1. While I prepared and analyzed the two-photon experiments, Irina Grigorova conducted the two-photon microscopy that is also presented in Figure 1. For the mapping of *ptcd*, I conducted the breeding, did the phenotyping, and genomic DNA isolation. Ying Xu assisted with some genomic DNA isolation and most SNP genotyping reactions. Olivia Lam assisted with some tail vein bleeding. Jinping An conducted sequencing reactions. This effort encompasses the bulk of Figure 2. The *koy* mouse was identified by Susan Watson during a collaborative screen with Chris Goodnow's lab in Australia. Together with Susan Watson and Craig Jenne, I characterized the *koy* mouse. I also further characterized the *ptcd* cells which encompasses the majority of Figure 3. David Roadcap, a postdoctoral fellow in James Bear's lab, conducted the actin biochemistry and recombinant Coro1A work presented in Figure 3H-K. Niko Foger provided the Coro1A-/- mice used for comparison. The patient samples were provided with Jennifer Puck, Kenneth Paris, and Ricardo Sorenson. Genechip analysis was generous provided by Pui Kwok's lab.

CHAPTER 1

Introduction

The adaptive immune response is dependent on a diverse T cell repertoire that traffics throughout the body to survey for foreign antigens. T cells are generated in the thymus, a critical lymphoid organ where precursor thymocytes develop to recognize foreign antigens by randomly rearranging their antigen receptors. While this random rearrangement generates enormous diversity, it also produces potentially auto-reactive thymocytes that are subsequently selected out. The surviving thymocytes further mature into T cells that exit the thymus to join the peripheral recirculating pool of T cells.

This pool of T cells recirculates between the blood, secondary lymphoid organs and the lymph (Figure 1A). Secondary lymphoid organs – including the spleen, lymph nodes, and Peyer's patches – serve as essential hubs for the initiation of immune responses (Figure 1B). T cells enter lymph nodes through specialized high-endothelial venules (HEVs) that display chemokines and adhesions molecules. Once inside the lymph node, T cells home to the T cell zone where they encounter dendritic cells (DCs) that present processed antigen. Each T cell will spend up to half a day within the lymph node scanning DCs for cognate antigen. If a T cell recognizes a cognate antigen, it will become activated and stay within the lymph node to initiate an immune response. Otherwise, the T cell will exit the lymph node and re-enter the circulation through lymphatic vessels.

This repetitive migration pattern ensures that the handful of T cells specific for any given antigen will sufficiently survey the entire body. Thus, exit from the thymus

and secondary lymphoid organs is critical for recirculation and immune surveillance. However, the mechanism for lymphocyte exit is poorly understood.

Transgenic studies with pertussis toxin (PTX)-expressing thymocytes resulted in an accumulation of mature thymocytes[1], suggesting that an active Gi-dependent process is required for thymic exit. FTY720, an immunosuppressive drug that blocks exit from both the thymus and peripheral lymphoid tissues[2], is structurally analogous to the sphingolipid sphingosine. Both FTY720 and sphingosine can be phosphorylated[2], and sphingosine-1-phosphate (S1P) is naturally abundant in circulating fluids[3]. These discoveries implicated the S1P family of G-protein coupled receptors in lymphocyte exit. Of the five S1P receptors, $S1P_1$ couples solely with G_i and binds FTY720-phosphate with high affinity[2].

The receptor $S1P_1$ is expressed on vascular endothelium as well as haematopoetic-derived cells and deletion of $S1P_1$ in mice is lethal at embryonic day 13.5 due to vascular defects[4]. Two approaches to restrict $S1P_1$ deficiency have demonstrated an intrinsic role for this receptor in lymphocyte exit. Bone marrow chimeras generated from $S1P_1$-/- fetal livers show a complete block in T and B lymphocyte egress from the thymus and peripheral lymphoid organs[5]. Also, a floxed allele of $S1P_1$ conditionally deleted in thymocytes causes an accumulation of mature thymocytes[6].

Genetic manipulations altering the tissue abundance of S1P also impairs lymphocyte egress. Levels of extracellular S1P are normally low in lymphoid tissues and high in the circulating fluids blood and lymph[3]. Pharmacological inhibition or knockdown of sphingosine lyase, an enzyme that degrades S1P, causes S1P levels to rise in lymphoid tissues and blocks lymphocyte egress[7]. Genetic ablation of the sphingosine kinases, required for phosphorylation of sphingosine, results in undetectable S1P in circulating fluids[8]. As with disrupting the sphingosine lyase, deleting both kinases inhibits lymphocyte egress. Together, these studies demonstrate the need for high S1P at egress sites and low tissue S1P for proper lymphocyte egress.

$S1P_1$ is highly sensitive to receptor modulation by S1P, and the surface expression of S1P1 on lymphocytes inversely correlates with S1P abundance in tissues[9]. After entering the lymph node, T lymphocytes recover their surface expression of $S1P_1$[9]. Following antigen-induced activation, T lymphocytes strongly downregulate $S1P_1$ transcript abundance[5]. Thus, $S1P_1$ surface expression can account for the behavior of lymphocytes during recirculation. After naïve T cells enter lymphoid tissues, $S1P_1$ levels recover over time and cells respond to high levels of S1P in circulating fluids to exit. But if the T cell encounters cognate antigen, it will downregulate $S1P_1$ transcripts and remain to mount an immune response. However, this antigen-induced transcriptional change occurs over days and is not sufficient to account for an acute blockade in lymphocyte egress, such as the lymph node "shutdown" effect.

The lymph node "shutdown" effect was first described in the 1960's by Hall and Morris when they observed a dramatic drop in the number of cells draining the popliteal lymph node following antigen injection in the legs of sheep[10]. Multiple studies in the following decades have replicated this observation in other animal models using various innate immune stimuli, such as type I interferons and tumor necrosis factor[11-14]. This transient process occurs rapidly to increase lymphocyte numbers in locally responding nodes. Thus innate immune stimuli can quickly signal the lymph node to accumulate more lymphocytes before antigen is available for presentation in the node. However, the mechanism for how these stimuli rapidly mediate this lymphocyte trafficking phenomenon was unknown.

In 1988, multiple groups described an antigen rapidly induced on the surface of hematopoetic cells by activation stimuli[15-19]. This molecule, now known as CD69, is a type II C-type lectin that shares homology most closely with natural killer (NK) receptors[20]. In both mouse and human genomes, CD69 is located within the NK complex[21, 22]. Unlike NK receptors, CD69 lacks any known signaling motifs on its cytoplasmic tail. Despite a broad expression pattern in many hematopoetics cell types, no ligand for CD69 has been reported. Studies using monoclonal antibodies (mAb) against CD69 to trigger signaling events in various hematopoetic cell types have produced conflicting conclusions on whether CD69 is a stimulatory or inhibitory receptor. However, the physiological relevance of these mAb-dependent studies is

questionable and their conclusions are based on a paradigm that CD69 signals and functions like NK receptors.

Initial genetic studies in mice did not reveal a clear function for CD69. CD69-/- mice lacked any overt phenotype[23]. Follow up studies on immune responses in CD69-/- mice produced conflicting results: with one set of studies attenuating an arthritis model with CD69-/- mice[24], and another set of studies reporting an increased immune response with CD69-/- mice in arthritis and tumor models[25, 26]. Two separate studies used transgenic mice to overexpress CD69 in thymocytes and resulted in mature thymocyte accumulation[27, 28]. These findings linked CD69 to a migration phenotype and hinted at a potential role in egress.

Various reports further linked CD69 with $S1P_1$. On the surface of $S1P_1$-/- lymphocytes, CD69 is uniformly expressed, but at a level less than that found on activated lymphocytes[5]. Also, FTY720 can rapidly induce CD69 downmodulation on maturing thymocytes[29]. Finally, $S1P_1$ was identified during a screen for inhibitors of T cell activation with CD69 induction as the assay measurement[30]. Together, these reports hinted at a cross-inhibitory interaction between CD69 and $S1P_1$.

In Chapter 2, we provide evidence for this association, and show that CD69 functions to inhibit $S1P_1$ and to rapidly block lymphocyte egress. This study allows us to assign a regulatory function for CD69 in lymphocyte trafficking. However, the

mechanism of $S1P_1$ in lymphocyte egress remains unclear. To understand the requirements for egress, we studied the spontaneous thymic egress mutant strain Cataract Shionogi (CTS).

The CTS strain was derived from a single spontaneous mutant mouse exhibiting small eyes and cataracts in an inbred colony of ICR mice at the Japanese company Shionogi[31]. The CTS strain was found to be T cell deficient after it failed to reject a graft from the related but MHC-mismatched non-obese diabetic (NOD) strain[32]. This T cell deficiency was attributed to a thymic egress defect[33] that was subsequently mapped to the distal end of chromosome 7[34]. This region of chromosome 7, named *ptcd* (peripheral T cell deficiency) lacked any genes known to be involved in lymphocytes egress.

In Chapter 3, we further characterize an intrinsic T cell migration and trafficking defect in *ptcd* mice. At the *ptcd* locus, we find a mutation in the actin regulator Coronin-1A that disrupts T cell trafficking.

References:

1. Chaffin, K. E. & Perlmutter, R. M. A pertussis toxin-sensitive process controls thymocyte emigration. Eur J Immunol 21, 2565-73 (1991).

2. Cyster, J. G. Chemokines, sphingosine-1-phosphate, and cell migration in secondary lymphoid organs. Annu Rev Immunol 23, 127-59 (2005).

3. Schwab, S. R. & Cyster, J. G. Finding a way out: lymphocyte egress from lymphoid organs. Nat Immunol 8, 1295-301 (2007).

4. Liu, Y. et al. Edg-1, the G protein-coupled receptor for sphingosine-1-phosphate, is essential for vascular maturation. J Clin Invest 106, 951-61 (2000).

5. Matloubian, M. et al. Lymphocyte egress from thymus and peripheral lymphoid organs is dependent on S1P receptor 1. Nature 427, 355-60 (2004).

6. Allende, M. L., Dreier, J. L., Mandala, S. & Proia, R. L. Expression of the sphingosine 1-phosphate receptor, S1P1, on T-cells controls thymic emigration. J Biol Chem 279, 15396-401 (2004).

7. Schwab, S. R. et al. Lymphocyte sequestration through S1P lyase inhibition and disruption of S1P gradients. Science 309, 1735-9 (2005).

8. Pappu, R. et al. Promotion of lymphocyte egress into blood and lymph by distinct sources of sphingosine-1-phosphate. Science 316, 295-8 (2007).

9. Lo, C. G., Xu, Y., Proia, R. L. & Cyster, J. G. Cyclical modulation of sphingosine-1-phosphate receptor 1 surface expression during lymphocyte recirculation and relationship to lymphoid organ transit. J Exp Med 201, 291-301 (2005).

10. Hall, J. G. & Morris, B. The immediate effect of antigens on the cell output of a lymph node. Br J Exp Pathol 46, 450-4 (1965).

11. Degre, M. Influence of polyinosinic: polycytidylic acid on the circulating white blood cells in mice. Proc Soc Exp Biol Med 142, 1087-91 (1973).

12. Korngold, R., Blank, K. J. & Murasko, D. M. Effect of interferon on thoracic duct lymphocyte output: induction with either poly I:poly C or vaccinia virus. J Immunol 130, 2236-40 (1983).

13. Kalaaji, A. N., Abernethy, N. J., McCullough, K. & Hay, J. B. Recombinant bovine interferon-alpha I 1 inhibits the migration of lymphocytes from lymph nodes but not into lymph nodes. Reg Immunol 1, 56-61 (1988).

14. Young, A. J., Seabrook, T. J., Marston, W. L., Dudler, L. & Hay, J. B. A role for lymphatic endothelium in the sequestration of recirculating gamma delta T cells in TNF-alpha-stimulated lymph nodes. Eur J Immunol 30, 327-34 (2000).

15. Lanier, L. L. et al. Interleukin 2 activation of natural killer cells rapidly induces the expression and phosphorylation of the Leu-23 activation antigen. J Exp Med 167, 1572-85 (1988).

16. Testi, R., Phillips, J. H. & Lanier, L. L. Constitutive expression of a phosphorylated activation antigen (Leu 23) by CD3bright human thymocytes. J Immunol 141, 2557-63 (1988).

17. Cebrian, M. et al. Triggering of T cell proliferation through AIM, an activation inducer molecule expressed on activated human lymphocytes. J Exp Med 168, 1621-37 (1988).

18. Naquet, P. et al. A novel T cell-activating molecule (THAM) highly expressed on CD4-CD8- murine thymocytes. J Immunol 141, 4101-9 (1988).

19. Bjorndahl, J. M., Nakamura, S., Hara, T., Jung, L. K. & Fu, S. M. The 28-kDa/32-kDa activation antigen EA 1. Further characterization and signal requirements for its expression. J Immunol 141, 4094-100 (1988).

20. Sancho, D., Gomez, M. & Sanchez-Madrid, F. CD69 is an immunoregulatory molecule induced following activation. Trends Immunol 26, 136-40 (2005).

21. Schnittger, S. et al. Regional sublocalization of the human CD69 gene to chromosome bands 12p12.3-p13.2, the predicted region of the human natural killer cell gene complex. Eur J Immunol 23, 2711-3 (1993).

22. Ziegler, S. F. et al. The mouse CD69 gene. Structure, expression, and mapping to the NK gene complex. J Immunol 152, 1228-36 (1994).

23. Lauzurica, P. et al. Phenotypic and functional characteristics of hematopoietic cell lineages in CD69-deficient mice. Blood 95, 2312-20 (2000).

24. Murata, K. et al. CD69-null mice protected from arthritis induced with anti-type II collagen antibodies. Int Immunol 15, 987-92 (2003).

25. Esplugues, E. et al. Enhanced antitumor immunity in mice deficient in CD69. J Exp Med 197, 1093-106 (2003).

26. Sancho, D. et al. CD69 downregulates autoimmune reactivity through active transforming growth factor-beta production in collagen-induced arthritis. J Clin Invest 112, 872-82 (2003).

27. Nakayama, T. et al. The generation of mature, single-positive thymocytes in vivo is dysregulated by CD69 blockade or overexpression. J Immunol 168, 87-94 (2002).

28. Feng, C. et al. A potential role for CD69 in thymocyte emigration. Int Immunol 14, 535-44 (2002).

29. Rosen, H., Alfonso, C., Surh, C. D. & McHeyzer-Williams, M. G. Rapid induction of medullary thymocyte phenotypic maturation and egress inhibition by nanomolar sphingosine 1-phosphate receptor agonist. Proc Natl Acad Sci U S A 100, 10907-12 (2003).

30. Chu, P. et al. Systematic identification of regulatory proteins critical for T-cell activation. J Biol 2, 21 (2003).

31. Ohotori, H., Yoshida, T. & Inuta, T. "Small eyes and cataract," a new dominant mutation in the mouse. Exp. Anim. 17, 91-6 (1968).

32. Makino, S., Muraoka, Y., Harada, M., Kishimoto, Y. & Konishi, T. in Diabetes 1988: Proceeding of the 13th Congress of the International Diabetes Federation (eds. Larkins, R., Zimmet, P. & Chishold, D.) 747-750 (Science Publishers B.V., 1989).

33. Yagi, H. et al. Defect of thymocyte emigration in a T cell deficiency strain (CTS) of the mouse. J Immunol 157, 3412-9 (1996).

34. Kimura, S. et al. Genetic control of peripheral T-cell deficiency in the cataract Shionogi (CTS) mouse linked to chromosome 7. Immunogenetics 47, 278-80 (1998).

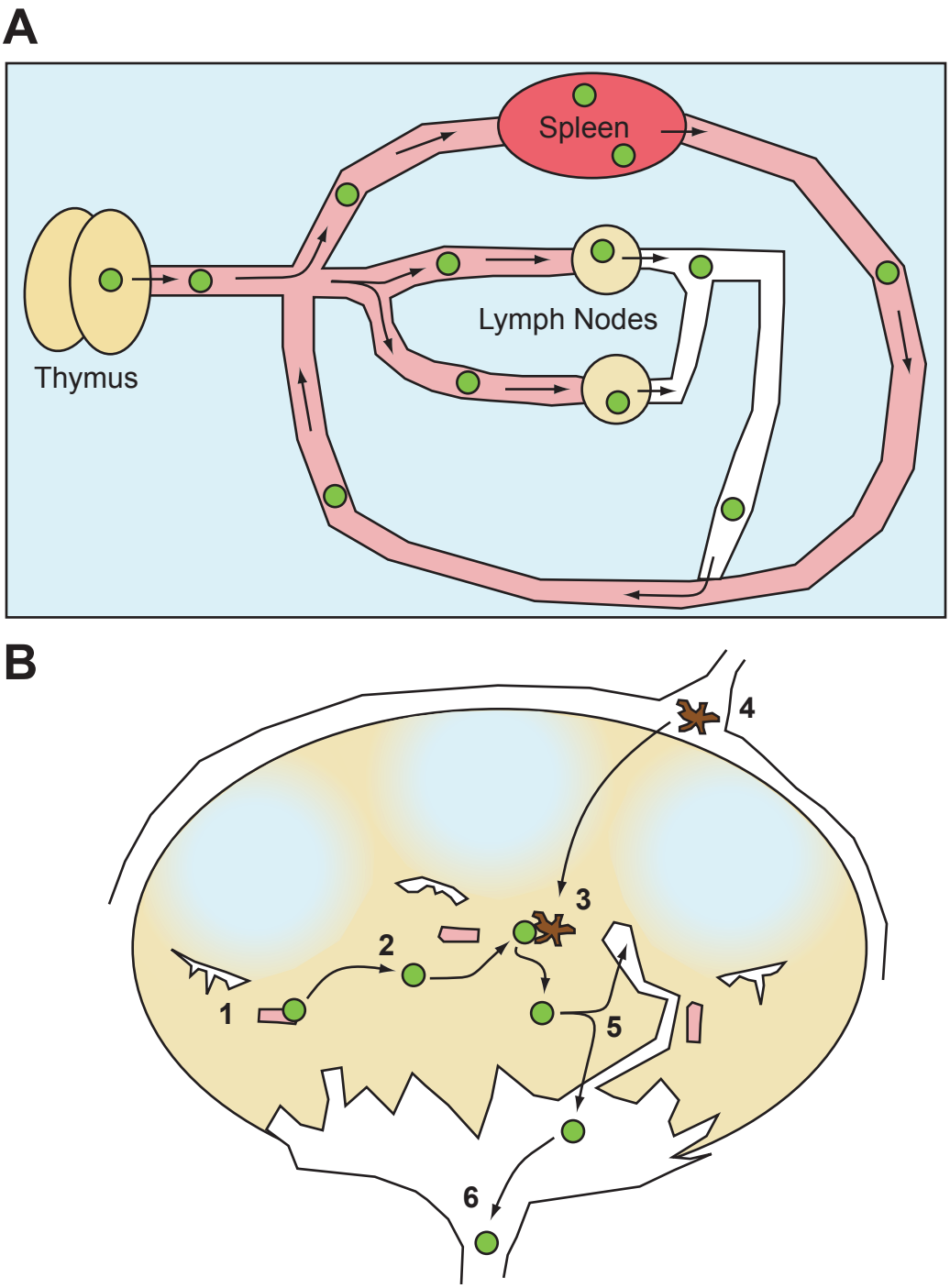

Figure 1. A. Schematic of T cell recirculation starting with exit from thymus. **B.** Example of T cell migration through lymph nodes: (1) Entry through HEV, (2) migration to T zone, (3) encounter with DC that (4) homes from peripheral tissue, and (5) exit via cortical or medullary sinuses into (6) efferent lymphatics.

CHAPTER 2

CD69 acts downstream of interferon-α/β to inhibit $S1P_1$ and lymphocyte egress from lymphoid organs

Shiow LR, Rosen DB, Brdickova N, Xu Y, An J, Lanier LL, Cyster JG, and Matloubian M, CD69 acts downstream of interferon-α/β to inhibit $S1P_1$ and lymphocyte egress from lymphoid organs (2006) *Nature,* 440(7083): 540-4

Abstract

Naive lymphocytes continually enter and exit lymphoid organs in a recirculation process that is essential for immune surveillance. During immune responses, the egress process can be shut down transiently[1]. When this occurs locally it increases lymphocyte numbers in the responding lymphoid organ; when it occurs systemically it can lead to immunosuppression as a result of the depletion of recirculating lymphocytes. Several mediators of the innate immune system are known to cause shutdown, including interferon α/β (IFN-α/β) and tumour necrosis factor[2–5], but the mechanism has been unclear. Here we show that treatment with the IFN-α/β inducer polyinosine•polycytosine (hereafter 'poly(I:C)') inhibited egress by a mechanism that was partly lymphocyte-intrinsic. The transmembrane C-type lectin CD69 was rapidly induced and *CD69-/-* cells were poorly retained in lymphoid tissues after treatment with poly(I:C) or infection with lymphocytic choriomeningitis virus. Lymphocyte egress requires sphingosine 1-phosphate receptor-1 ($S1P_1$), and IFN-α/β was found to inhibit lymphocyte responsiveness to S1P. By contrast, *CD69-/-* cells retained $S1P_1$ function after exposure to IFN-α/β. In coexpression experiments, CD69 inhibited $S1P_1$ chemotactic function and led to downmodulation of $S1P_1$. In a reporter assay, $S1P_1$ crosslinking led to co-crosslinking and activation of a CD69–CD3ζ chimaera. CD69 co-immunoprecipitated with $S1P_1$ but not the related receptor, $S1P_3$. These observations indicate that CD69 forms a complex with and negatively regulates $S1P_1$ and that it functions downstream of IFN-α/β, and possibly other activating stimuli, to promote lymphocyte retention in lymphoid organs.

Introduction, Results and Discussion

When mice were treated with poly(I:C), a double-stranded RNA mimetic, we observed that lymphocyte numbers in blood and lymph decreased rapidly, reaching a minimum by 6 h (Fig. 1a, and Supplementary Fig. 1a). This effect was largely mediated by IFN-α/β because mice deficient in IFN-α/β-receptor-1 (IFNAR1) showed only a weak response (Fig. 1b). The effect of IFN-α/β was, in part, lymphocyte-intrinsic because adoptively transferred *Ifnar1*$^{-/-}$ lymphocytes were less efficiently sequestered than wild-type cells after treatment with poly(I:C) (Fig. 1c, and Supplementary Fig. 1b). In particular, *Ifnar1*$^{-/-}$ T cells egressed into the lymph of poly(I:C)-treated animals in fourfold greater numbers than wild-type control cells present in the same animals, and *Ifnar1*$^{-/-}$ B cells entered the lymph in sixfold to sevenfold greater numbers (Fig. 1c, d).

The recent finding that $S1P_1$, a G-protein-coupled receptor (GPCR), is required within lymphocytes for egress from lymphoid organs[6,7] led us to ask whether IFNAR1 signalling altered lymphocyte S1P responsiveness. In chemotaxis assays, T lymphocytes taken from mice that had been pretreated with poly(I:C) showed markedly reduced responsiveness to S1P (Fig. 1e). Lymphocytes that lacked IFNAR1 were largely resistant to this effect, indicating that it was due to intrinsic IFNAR1 signalling (Fig. 1e). Although B cells migrate poorly to S1P directly *ex vivo*, they acquire increased chemotactic responsiveness after several hours *in vitro* incubation (Fig. 1f). Exposure of the splenocyte cultures to poly(I:C) or to recombinant IFN-α/β inhibited the B-cell

response to S1P (Fig. 1f). In contrast with the marked loss of S1P chemotactic responsiveness, quantitative polymerase chain reaction (PCR) analysis showed that $S1P_1$ mRNA was only partly decreased in abundance in T and B cells from poly(I:C)-treated mice (Fig. 1g).

IFN-α/β is a strong inducer of the cell surface activation marker, CD69 (Fig. 2a). In two independent studies, it was found that transgenic overexpression of CD69 causes decreased egress of mature single-positive T cells from the thymus[8,9]. However, CD69-deficient mice had normal thymic egress, calling into question the physiological relevance of the transgenic studies[10,11]. We tested whether CD69 might be involved in the IFNAR1-mediated inhibition of lymphocyte egress by transferring wild-type and *CD69-/-* cells into wild-type hosts and treating them with poly(I:C). Whereas transferred wild-type cells were almost undetectable in the lymph 6 h after treatment with poly(I:C), *CD69-/-* cells continued to appear in the lymph (Fig. 2b). Similarly, the sequestration and depletion of T and B lymphocytes from blood was less complete for *CD69-/-* cells than for wild-type cells (Supplementary Fig. 2a). Quantitative PCR analysis for interferon response factor (IRF)-7 confirmed that the *CD69-/-* and wild-type cells were similarly activated (Supplementary Fig. 2b) and $S1P_1$ mRNA abundance was reduced to the same extent as that observed in wild-type cells (Supplementary Fig. 2c). These observations showed that CD69 is required downstream of IFNAR1 to inhibit lymphocyte egress. Lymphocytic choriomeningitis virus (LCMV) infection also caused a decrease in T-cell

and B-cell numbers in lymph and blood, and this effect was strongly inhibited when the lymphocytes lacked CD69 (Fig. 2c, and Supplementary Fig. 3a, b).

In contrast to wild-type T cells, *CD69-/-* T cells retained a substantial fraction of their S1P responsiveness after treatment with poly(I:C) (Fig. 2d). Similarly, *CD69-/-* B cells exposed to IFN-α/β *in vitro* retained much of their S1P responsiveness (Fig. 2d). By flow cytometric analysis, $S1P_1$ was downregulated from the surface of wild-type T cells but was only partly downregulated on *CD69-/-* T cells after treatment with poly(I:C) (Fig. 2e) or infection with LCMV (Supplementary Fig. 3c). These observations indicated that CD69 might be required for maximal $S1P_1$ downmodulation.

To further characterize the mechanism of CD69-mediated inhibition of $S1P_1$, we used a co-transfection approach in the WEHI-231 B-cell line. Cells were transduced with a retrovirus encoding Flag-tagged mouse $S1P_1$, an internal ribosomal entry site (IRES) and cytoplasmic-domain truncated human CD4 (hCD4) as a reporter. These cells expressed the Flag-tagged receptor on the surface in amounts proportional to the amount of hCD4 expressed (Fig. 3a). Similarly, cells transduced with a mouse CD69–IRES-green fluorescent protein (GFP) construct expressed CD69 on the surface in proportion to the amount of GFP expressed (Fig. 4a). However, when the CD69–IRES-GFP retrovirus was introduced into the Flag-$S1P_1$-expressing cells, there was a loss of surface Flag-$S1P_1$ staining in cells expressing the highest amounts of GFP (Fig. 3a, b), and in chemotaxis assays these cells showed little response to S1P but retained responsiveness to the

chemokine SDF1 (CXCL12) (Fig. 3c). Co-transduction of Flag-$S1P_1$-expressing cells with another C-type lectin, mouse CD23, did not lead to downmodulation of surface expression and did not affect the function of $S1P_1$ (Fig. 3b,c). When CD69 was introduced into cells expressing Flag-$S1P_3$, the receptor was not downmodulated (Fig. 3b). These findings indicate that in cells with abundant CD69, $S1P_1$ is selectively downmodulated and functionally inhibited.

Although CD69 has been well studied as a lymphocyte activation marker and is transcriptionally induced by many activation stimuli[12,13], naive CD69-surface negative lymphocytes express considerable amounts of basal CD69 mRNA (Figs 2a and 3d) and have detectable intracellular CD69 protein[14]. In $S1P_1$-deficient B and T cells, CD69 is found on the cell surface, although these cells do not express other activation markers or show evidence of increased cell size[6,15]. Moreover, $S1P_1$-deficient B and T cells have the same amounts of CD69 mRNA as control B and T cells (Fig. 3d). These findings indicate that in naive wild-type lymphocytes the small amounts of CD69 that are expressed might be prevented from surface expression by $S1P_1$. Indeed, when we plotted Flag-$S1P_1$ against CD69 in total GFP^+ $hCD4^+$ co-transduced WEHI-231 cells we observed that there was mutual exclusion of surface expression (Fig. 3e). The $CD69^+$ Flag-$S1P_1^-$ cells (Fig. 3e, region 1) expressed high levels of GFP (Fig. 3a, b); by contrast, cells expressing only Flag-$S1P_1$ on the surface were GFP^{low} (Fig. 3e, region 2 and inset). CD69 was readily detectable on the surface of GFP^{low} cells after transduction with the CD69 construct alone (Fig. 3f). Thus, in addition to the inhibitory effect of high CD69 expression on surface

Flag-$S1P_1$ levels, there was an inhibitory effect of $S1P_1$ on surface CD69 expression when the abundance of CD69 was low. This effect was specific for CD69 and $S1P_1$ because CD69 and $S1P_3$ were coexpressed on the surface of cells without any evidence of cross-inhibition (Fig. 3g). In concordance with these observations, human $S1P_1$ was identified in a retroviral cDNA library overexpression screen as a suppressor of human CD69 surface expression[16]. $S1P_1$ is a $G_{i\alpha}$-coupled receptor[17], and treatment of the cells co-transduced with $S1P_1$ and CD69 for 6 h with pertussis toxin, a $G_{i\alpha}$ inhibitor, led to partial recovery of CD69 surface expression in the $S1P_1^+$ GFP^{low} cells (Fig. 3e, h). Thus, $S1P_1$-mediated modulation of CD69 was at least partly dependent on $G_{i\alpha}$ signalling. Agonist-induced downmodulation might account for the ability of the S1P receptor agonist FTY720-phosphate to cause CD69 downmodulation in single-positive thymocytes[18] that normally reside in an S1P-poor environment[19].

To test further for an association between CD69 and $S1P_1$, 2B4 T lymphoma cells expressing an nuclear factor of activated T cells (NFAT)-GFP reporter[20] were transduced with a mouse CD69 ectodomain and transmembrane domain plus human CD3ζ cytoplasmic domain fusion protein (CD69–CD3ζ) alone or together with Flag-tagged $S1P_1$. In this assay, GFP expression is induced after CD3ζ cytoplasmic domain cross-linking and, as expected, GFP induction was observed after treatment of the CD69–CD3ζ-transduced cells with anti-CD69 antibodies (Fig. 4a). GFP induction was also observed after anti-Flag antibody treatment of cells co-transduced with CD69–CD3ζ and Flag-$S1P_1$, whereas no GFP induction occurred after anti-Flag treatment of cells

transduced with Flag-$S1P_1$ alone (Fig. 4a). In cells transduced with Flag-$S1P_3$ and CD69–CD3ζ, no GFP induction occurred after treatment with anti-Flag antibody (Fig. 3a). Flow cytometric analysis demonstrated that the CD69–CD3ζ chimaera was coexpressed on the cell surface together with Flag-$S1P_1$ (Supplementary Fig. 4a). This was also observed when WEHI231 cells were co-transduced with these constructs (Supplementary Fig. 4b), indicating that the intact CD69 cytoplasmic domain is needed for efficient downmodulation of the coexpressed molecules from the cell surface. These findings indicate that antibody-mediated crosslinking of Flag-$S1P_1$ led to co-crosslinking and activation of CD69–CD3ζ, providing further evidence that these molecules closely associate on the membrane and indicating that the CD69 ectodomain and transmembrane domains are sufficient to mediate this association.

As a further approach to test whether $S1P_1$ and CD69 formed a complex, we examined whether these molecules could be coimmunoprecipitated. Using lysates prepared from co-transduced WEHI231 B cells we found that mouse CD69 co-precipitated with Flag-$S1P_1$, whereas another C-type lectin, CD23, did not (Fig. 4b). CD69 failed to co-immunoprecipitate with Flag-$S1P_3$ (Fig. 4b). Mouse CD69, CD23, $S1P_1$ and $S1P_3$ have N-linked glycosylation sites, and the broad band detected for each molecule in western blot analysis is most probably due to the glycosylation. To test whether an association also occurred between human CD69 and $S1P_1$, we prepared lysates from Jurkat T lymphoma cells that had been transduced with epitope-tagged human $S1P_1$ and stimulated with anti-T cell receptor antibody to promote the

upregulation of CD69. Immunoprecipitation of endogenous CD69 was found to co-immunoprecipitate epitope-tagged $S1P_1$ and vice versa (Fig. 4c). Although not excluding the involvement of additional molecules, these findings provide evidence for an evolutionarily conserved interaction between CD69 and $S1P_1$ in lymphocytes.

Our observations indicate that CD69, a type II transmembrane protein, might engage in a novel mode of GPCR negative regulation by forming a complex with $S1P_1$, promoting downmodulation and inhibiting the function of this receptor in lymphocyte egress. In addition to IFN-α/β, CD69 transcription is induced in response to most stimuli that cause lymphocyte activation, including other stimuli that are known to cause lymphocyte sequestration, such as tumour necrosis factor and antigen stimulation[5,12,21]. Activating stimuli can also cause $S1P_1$ transcriptional downregulation[6,22] and this would be expected to decrease the amounts of CD69 needed to dominate and inhibit any remaining $S1P_1$. Consistent with CD69 functioning to promote sequestration of human lymphocytes was the observation that human *CD69-/-* T cells are rare in blood compared with lymphoid tissues and inflammatory sites[12]. In addition to lymphocyte-intrinsic effects, our findings indicate that IFN-α/β has extrinsic effects that regulate egress. CD69 deficiency has been associated with augmented anti-tumour responses and the development of exaggerated collagen-induced arthritis[13]. This has been suggested to be due to altered production of transforming growth factor-β[23], but altered trafficking of activated lymphocytes may also be involved. We speculate that in some cell types, $S1P_1$ and CD69 may be coexpressed as a non-modulating complex and that this might allow CD69 signalling through associated $S1P_1$ molecules. In this regard, it is notable that

CD69 has been found to be associated with a heterotrimeric G protein[14] and that some effects of CD69 cross-linking antibodies are sensitive to pertussis toxin[24–26]. $S1P_1$ is currently being targeted by small molecules as a mechanism of inducing lymphocyte sequestration and immunosuppression[17,27]. Therapeutic augmentation of CD69 levels may be a new method for regulating $S1P_1$ function in lymphoid cells.

Methods

Mice, adoptive transfers and treatments

C57BL/6 (B6) and B6-CD45.1 mice were obtained from the National Cancer Institute. *Ifnar1*$^{-/-}$ mice[28] were ten generations and *CD69*$^{-/-}$ mice[11] six generations backcrossed to B6 mice. S1P$_1^{-/-}$ thymocytes and B cells were generated as described previously[6]. For adoptive transfers, spleen and lymph node cells were labelled with either 1 μM 5-(and-6)-(((4-chloromethyl)benzoyl)amino)tetramethylrhodamine (CMTMR; Molecular Probes) or 1 μM 5-(and6-)-carboxyfluorescein diacetate succinimidyl ester (CFSE; Molecular Probes)[29] and mixed together or with wild-type control CD45.1 lymphocytes and injected intravenously into recipients. After 36–40 h, mice were injected intravenously with 100 μg of poly(I:C) (Sigma) or an equivalent volume of saline. Treatment with poly(I:C) was for 6 h unless otherwise indicated. For infection with LCMV, 2×10^6 plaque-forming units of Armstrong strain were injected intravenously 24 h after adoptive transfer. Lymph collection was as described previously[6]. Statistical analysis was with a paired two-tailed Student's *t*-test.

Flow cytometry, transwell migration assays, cell purification and quantitative PCR

Procedures were similar to those described previously[6,15,29] and are detailed in Supplementary Methods.

Constructs and retroviral transduction

Details on MSCV2.2 retroviral constructs and transduction procedures are provided in Supplementary Methods. Quantitative PCR analysis of total $S1P_1$ and CD69 transcript abundance in two preparations of co-transduced WEHI231 cells showed they were within fivefold of the levels in T cells isolated from mice 6 h after treatment with poly(I:C).

Reporter cell assay

2B4 cells containing an NFAT-GFP reporter were transduced and analysed as described previously[20,30].

Immunoprecipitation

Transduced WEHI231 cells were lysed in 0.875% Brij 97, 0.125% Nonidet P40, 150 mM NaCl, 10 mM Tris-HCl pH 7.4, 0.02% NaN_3 buffer containing protease inhibitors (Sigma). Transfected Jurkat cells were stimulated or not with anti-Jurkat TCR Vb antibody C305 (ascites diluted 1:1,000) and lysed with 1% n-dodecyl-b-D-maltoside (Calbiochem) in 20 mM Tris-HCl pH 7.5 containing 100 mM NaCl, 10 mM EDTA, 50 mM NaF and 1 mM Pefabloc. Immunoprecipitation was by standard procedures as described in Supplementary Methods.

Supplementary Materials and Methods

Flow cytometry and Chemotaxis

Data were acquired on a FACSCalibur or LSRII (Becton Dickinson) and analyzed with FlowJo software (Treestar). Fluorochrome- or biotin-conjugated antibodies were from BD Pharmingen or eBioscience. Affinity-purified $S1P_1$ specific and control rabbit antiserum were generated as described[29]. Chemotaxis was across bare 5 μm Transwell filters (Corning Costar Corp.) over 3 h in response to S1P (Sigma) or SDF1 (Preprotech) as described[6]. Recombinant murine IFNa was from PBL Laboratories.

Cell purification and PCR

T and B cells were purified from spleen and lymph node cells[29,6] using an autoMACS (Miltenyi Biotec) resulting in purities of at least 95%. Purification of *CD69*$^{-/-}$ T and B cells and fetal liver chimera thymocytes and B cells was on a FACSAria (BD) or MoFlo sorter (Dako Cytomation), resulting in purities of at least 99%. Quantitative PCR on an ABI 7700 sequence detection instrument (Taqman; PE Applied Biosystems) was as described using reported primer/probe sets[6], and CD69 forward primer TGGTCCTCATCACGTCCTTAATAA, reverse primer TCCAACTTCTCGTACAAGCCTG, probe CATTGCCTTAAATGTGGGCAAGTACAATTGC; and IRF7 forward primer GCTTGGATCTACTGTGGGC, reverse primer CACGGTCTTGCTCCTGGC and SYBR Green (Biorad). Data are shown as relative amount of the indicated messenger RNA normalized to HPRT.

Constructs and retroviral transduction

Construction of the MSCV2.2 retroviral vector expressing a FLAG-tagged full-length mouse $S1P_1$, upstream of an IRES and a cytoplasmic domain-truncated human CD4, has been described[29]. Full-length mouse $S1P_3$ was also cloned into this vector. Mouse CD23 and CD69 were cloned from splenic cDNA into MSCV2.2 upstream of an IRES and GFP element. The ecto- and transmembrane domains of mouse CD69 (residues 31-197) were cloned into a pMX-puro retroviral vector containing the cytoplasmic domain of human CD3z introduced onto the N-terminus of the chimeric receptor[6]. Cultures of Bosc23 packaging cell line were transfected with the constructs and supernatants containing retrovirus were collected, and WEHI-231 and 2B4 cells were infected as described[29].

Immunoprecipitaton

WEHI-231 cells were stably transduced with FLAG-$S1P_1$-IRES-hCD4 or FLAG-$S1P_3$-IRES-hCD4, and HA-CD23-IRES-GFP or HA-CD69-IRES-GFP. $2x10^7$ WEHI231 cells of each population were washed in PBS and lysed in 1 mL lysis buffer (0.875% Brij 97, 0.125% NP-40, 150mM NaCl, 10 mM Tris-HCl pH7.4, 0.02% NaN3) containing protease inhibitors (Sigma) for 30 min on ice. Postnuclear supernatants were precleared before incubation with EZView FLAG M2 beads (Sigma) for 1 h. Beads were stringently washed with lysis buffer containing 1.5M NaCl. Samples were eluted and reduced before separation by 10% SDS-PAGE and blotting using biotinylated anti-HA (Roche), anti-FLAG M1 (Sigma), anti-mouse HRP (Amersham), and streptavidin HRP (Jackson ImmunoResearch). $2x10^8$ transduced Jurkat cells grown in RPMI 5% FBS were

electroporated with 0.2 mg of either pEF.Myc.His.IRES.NGFR empty vector or pEF.S1P$_1$.Myc.His.IRES.NGFR which contains a human S1P$_1$ insert with a C-terminal Myc epitope tag. 28 h later cells were stimulated or not with anti-Jurkat TCR Vb antibody C305 (1000x diluted ascites), overnight, to induce CD69 expression. Cells were washed in RPMI medium without FBS and incubated 30 min in RPMI with 0.5% BSA to upregulate S1P$_1$ on the surface. $7.5x10^7$ of the cells for each condition were then lysed in 0.75 ml lysis buffer (1% n-Dodecyl-beta-D-maltoside (Calbiochem) in 20 mM Tris pH 7.5 containing 100 mM NaCl, 10 mM EDTA, 50 mM NaF, 1mM Pefabloc) 30 min on ice. Postnuclear supernatants were subjected to I.P. with either anti-Myc antibody 9B11 (Cell signaling) or anti-CD69 antibody L78 (Becton Dickinson) and protein A or G sepharose, respectively. Nonreduced and reduced samples were analyzed by Western-blotting using goat anti-CD69 (R&D systems) and rabbit anti-Myc HRP (Santa Cruz) antibodies respectively.

Acknowledgements

We thank T. Nakayama and S. Zeigler for *CD69-/-* mice; K. Murali-Krishna for *IFNAR1-/-* mice; R. Proia for *S1P1+/-* mice; S. Jahn for technical assistance; C. Allen, S. Schwab and C. McArthur for help with cell-sorting; K. Kabashima for fetal liver chimeras; O. Lam for mouse husbandry; and S. Schwab and C. Lo for comments on the manuscript. L.R.S. is supported by the UCSF Medical Scientist Training Program; M.M. was supported by the Pfizer Postdoctoral Fellowship in Immunology and Rheumatology, a research award from the Arthritis Foundation, the Rosalind Russell Medical Research Center for Arthritis at UCSF, and the Sandler Family Supporting Foundation; L.L.L. is an American Cancer Society Research Professor; J.G.C. is an investigator of the Howard Hughes Medical Institute. This work was supported in part by grants from the NIH (to L.L.L. and J.G.C.).

References

1. Hall, J. G. & Morris, B. The immediate effect of antigens on the cell output of a lymph node. *Br. J. Exp. Pathol.* **46,** 450–454 (1965).

2. Degre, M. Influence of polyinosinic:polycytidylic acid on the circulating white blood cells in mice. *Proc. Soc. Exp. Biol. Med.* **142,** 1087–1091 (1973).

3. Korngold, R., Blank, K. J. & Murasko, D. M. Effect of interferon on thoracic duct lymphocyte output: induction with either poly I:poly C or vaccinia virus. *J. Immunol.* **130,** 2236–2240 (1983).

4. Kalaaji, A. N., Abernethy, N. J., McCullough, K. & Hay, J. B. Recombinant bovine interferon-alpha I 1 inhibits the migration of lymphocytes from lymph nodes but not into lymph nodes. *Reg. Immunol.* **1,** 56–61 (1988).

5. Young, A. J., Seabrook, T. J., Marston, W. L., Dudler, L. & Hay, J. B. A role for lymphatic endothelium in the sequestration of recirculating gamma delta T cells in TNF-alpha-stimulated lymph nodes. *Eur. J. Immunol.* **30,** 327–334 (2000).

6. Matloubian, M. *et al.* Lymphocyte egress from thymus and peripheral lymphoid organs is dependent on S1P receptor 1. *Nature* **427,** 355–360 (2004).

7. Allende, M. L., Dreier, J. L., Mandala, S. & Proia, R. L. Expression of the sphingosine-1-phosphate receptor, S1P1, on T-cells controls thymic emigration. *J. Biol. Chem.* **279,** 15396–15401 (2004).

8. Feng, C. *et al.* A potential role for CD69 in thymocyte emigration. *Int. Immunol.* **14,** 535–544 (2002).

9. Nakayama, T. *et al.* The generation of mature, single-positive thymocytes *in vivo* is dysregulated by CD69 blockade or overexpression. *J. Immunol.* **168,** 87–94 (2002).

10. Lauzurica, P. *et al.* Phenotypic and functional characteristics of hematopoietic cell lineages in CD69-deficient mice. *Blood* **95,** 2312–2320 (2000).

11. Murata, K. *et al.* CD69-null mice protected from arthritis induced with anti-type II collagen antibodies. *Int. Immunol.* **15,** 987–992 (2003).

12. Testi, R., D'Ambrosio, D., De Maria, R. & Santoni, A. The CD69 receptor: a multipurpose cell-surface trigger for hematopoietic cells. *Immunol. Today* **15,** 479–483 (1994).

13. Sancho, D., Gomez, M. & Sanchez-Madrid, F. CD69 is an immunoregulatory molecule induced following activation. *Trends Immunol.* **26,** 136–140 (2005).

14. Risso, A. *et al.* CD69 in resting and activated T lymphocytes. Its association with a GTP binding protein and biochemical requirements for its expression. *J. Immunol.* **146,** 4105–4114 (1991).

15. Cinamon, G. *et al.* Sphingosine 1-phosphate receptor 1 promotes B cell localization in the splenic marginal zone. *Nature Immunol.* **5,** 713–720 (2004).

16. Chu, P. *et al.* Systematic identification of regulatory proteins critical for T-cell activation. *J. Biol.* **2,** 21.1–21.16 (2003).

17. Brinkmann, V., Cyster, J. G. & Hla, T. FTY720: sphingosine 1-phosphate receptor-1 in the control of lymphocyte egress and endothelial barrier function. *Am. J. Transplant.* **4,** 1019–1025 (2004).

18. Rosen, H., Alfonso, C., Surh, C. D. & McHeyzer-Williams, M. G. Rapid induction of medullary thymocyte phenotypic maturation and egress inhibition by nanomolar sphingosine 1-phosphate receptor agonist. *Proc. Natl Acad. Sci. USA* **100,** 10907–10912 (2003).

19. Schwab, S. R. *et al.* Lymphocyte sequestration through S1P lyase inhibition and disruption of S1P gradients. *Science* **309,** 1735–1739 (2005).

20. Arase, H., Mocarski, E. S., Campbell, A. E., Hill, A. B. & Lanier, L. L. Direct recognition of cytomegalovirus by activating and inhibitory NK cell receptors. *Science* **296,** 1323–1326 (2002).

21. Lopez-Cabrera, M. *et al.* Transcriptional regulation of the gene encoding the human C-type lectin leukocyte receptor AIM/CD69 and functional characterization of its tumor necrosis factor-alpha-responsive elements. *J. Biol. Chem.* **270,** 21545–21551 (1995).

22. Graeler, M. & Goetzl, E. J. Activation-regulated expression and chemotactic function of sphingosine 1-phosphate receptors in mouse splenic T cells. *FASEB J.* **16,** 1874–1878 (2002).

23. Esplugues, E. *et al.* Enhanced antitumor immunity in mice deficient in CD69. *J. Exp. Med.* **197,** 1093–1106 (2003).

24. Ramirez, R., Carracedo, J., Zamzami, N., Castedo, M. & Kroemer, G. Pertussis toxin inhibits activation-induced cell death of human thymocytes, pre-B leukemia cells and monocytes. *J. Exp. Med.* **180,** 1147–1152 (1994).

25. Sancho, D. *et al.* Functional analysis of ligand-binding and signal transduction domains of CD69 and CD23 C-type lectin leukocyte receptors. *J. Immunol.* **165,** 3868–3875 (2000).

26. Bikah, G., Pogue-Caley, R. R., McHeyzer-Williams, L. J. & McHeyzer-Williams, M. G. Regulating T helper cell immunity through antigen responsiveness and calcium entry. *Nature Immunol.* **1,** 402–412 (2000).

27. Rosen, H. & Liao, J. Sphingosine 1-phosphate pathway therapeutics: a lipid ligand-receptor paradigm. *Curr. Opin. Chem. Biol.* **7,** 461–468 (2003).

28. Muller, U. *et al.* Functional role of type I and type II interferons in antiviral defense. *Science* **264,** 1918–1921 (1994).

29. Lo, C. G., Xu, Y., Proia, R. L. & Cyster, J. G. Cyclical modulation of sphingosine-1-phosphate receptor 1 surface expression during lymphocyte recirculation and relationship to lymphoid organ transit. *J. Exp. Med.* **201,** 291–301 (2005).

30. Rosen, D. B. *et al.* Cutting edge: Lectin-like transcript-1 is a ligand for the inhibitory human NKR-P1A receptor. *J. Immunol.* **175,** 7796–7799 (2005).

Figure 1 | Lymphocyte-intrinsic IFNAR1 requirement during poly(I:C)-induced lymphocyte sequestration and downregulation of $S1P_1$ by IFN-α/β. a, Mice were injected with phosphate-buffered saline (PBS) or poly(I:C) and at the indicated times B-cell and T-cell numbers in the lymph were determined. Results show means±s.d. for three poly(I:C)-treated mice per time point. The '0' h data are from mice injected 6 h earlier with PBS. Triangles, $CD19^+$; circles, $CD4^+$; squares, $CD8^+$. **b**, Wild-type mice (open columns) and *Ifnar1*$^{-/-}$ mice (filled columns) were treated with poly(I:C) for 6 h; cell frequency in lymph is shown as a percentage of the PBS-treated controls (*n*=4). **c**, **d**, Wild-type and IFNAR1-deficient lymphocytes were labelled with CFSE and CMTMR, respectively, and transferred into wild-type mice. At 6 h after treatment with poly(I:C) (filled columns) or PBS (open columns), lymph was analysed for the number of transferred cells (**c**) and the ratio of transferred IFNAR1-deficient cells to wild-type cells (**d**). Columns represent averages and open circles individual animals from two experiments, representative of five. **e**, Migration assay of transferred T cells from recipients treated as in **c**. Squares, *Ifnar1*$^{+/+}$; circles, *Ifnar1*$^{-/-}$; open symbols, PBS; filled symbols, poly(I:C). **f**, Migration assay of B cells from wild-type mice after incubation for 10 h in vehicle (diamonds), 20 μg ml^{-1} poly(I:C) (squares) or 1,000 U ml^{-1} IFN-α (circles). In **e** and **f**, data points show the mean of duplicates and bars the range for one of three experiments. **g**, Quantitative PCR analysis of $S1P_1$ in T and B cells from wild-type mice treated with poly(I:C) (filled columns) or PBS (open columns). Double-positive thymocytes from an untreated mouse are shown (grey column) as an example of cells lacking $S1P_1$ (ref. 6).

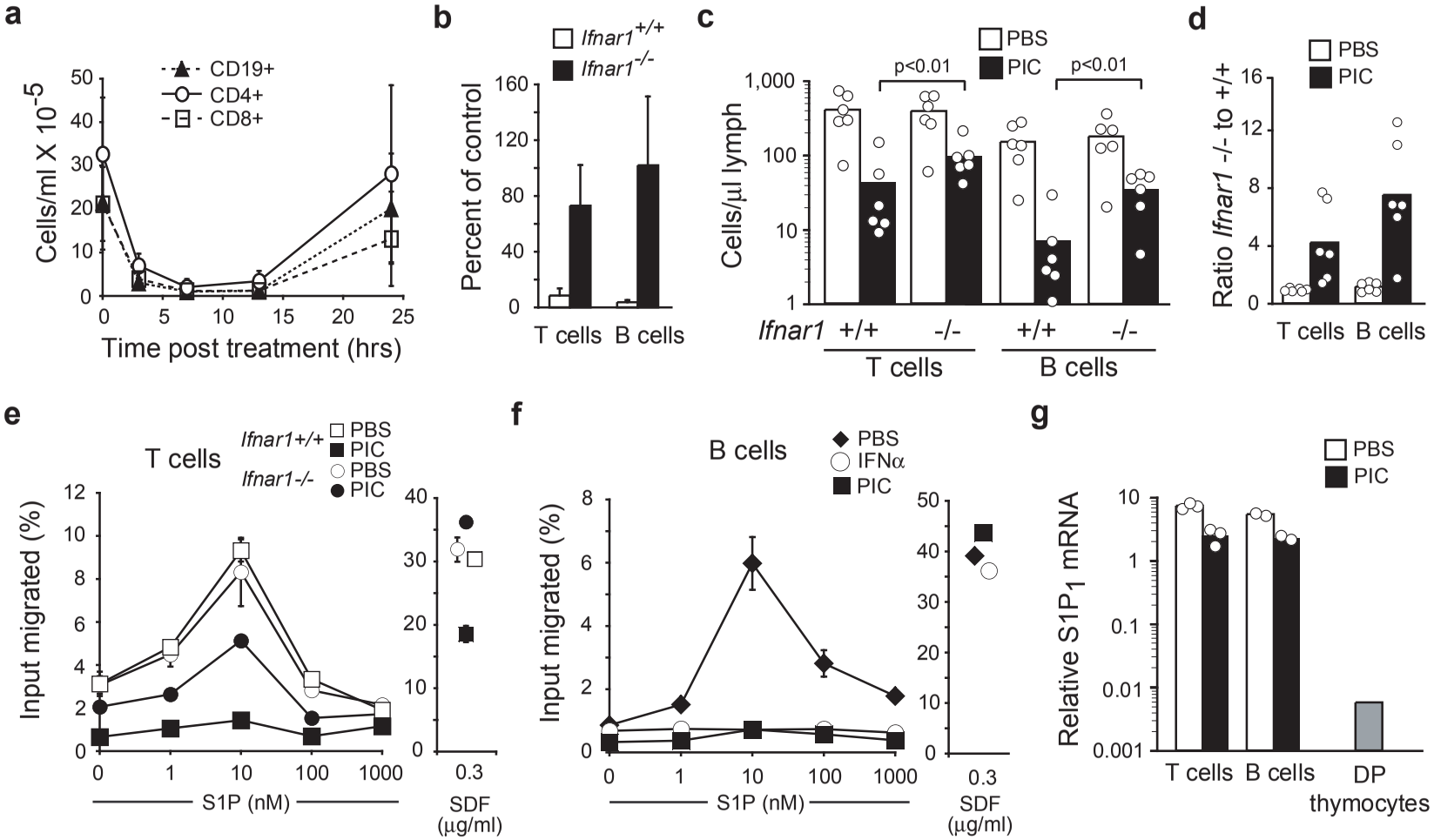
a
Cells/ml X 10-5
CD19+
CD4+
CD8+
Time post treatment (hrs)
b
Ifnar1+/+
Ifnar1-/-
Percent of control
T cells
B cells
c
PBS
PIC
p<0.01
p<0.01
Cells/µl lymph
Ifnar1 +/+ -/- +/+ -/-
T cells
B cells
d
PBS
PIC
Ratio Ifnar1 -/- to +/+
T cells
B cells
e
T cells
Ifnar1+/+ PBS
PIC
Ifnar1-/- PBS
PIC
Input migrated (%)
S1P (nM)
SDF (µg/ml)
f
B cells
PBS
IFNα
PIC
Input migrated (%)
S1P (nM)
SDF (µg/ml)
g
PBS
PIC
Relative S1P1 mRNA
T cells
B cells
DP thymocytes

Figure 1

Figure 2 | CD69-deficient cells are less efficiently sequestered after treatment with poly(I:C) and LCMV infection and retain S1P responsiveness. a, Quantitative PCR (left panel) and flow cytometric analysis (right panels) of CD69 in spleen T and B cells from mice treated with poly(I:C) (filled columns) or PBS (open columns). Staining of cells from PBS-treated mice was identical to the staining of *CD69*$^{-/-}$ cells (not shown). PIC, poly(I:C). **b**, Wild-type and CD69-deficient lymphocytes were labelled and transferred into recipient mice that were treated and analysed as in Fig. 1c. Filled columns, poly(I:C); open columns, PBS. **c**, Recipients of labelled wild-type and CD69-deficient lymphocytes were uninfected (open columns) or infected (filled columns) with LCMV and analysed at 18 h for cell numbers in lymph. Data are representative of three experiments. **d**, Left: migration assay of transferred T cells from recipients of wild-type (squares) and *CD69*$^{-/-}$ (circles) lymphocytes treated with PBS (open symbols) or poly(I:C) (filled symbols). Data are means±s.d. for nine mice from three experiments. Right: migration assay of B cells from wild-type (squares) and *CD69*$^{-/-}$ (circles) mice after incubation for 6 h in the absence (open symbols) or presence (filled symbols) of 1,000 U ml^{-1} IFN-α. Data are from one experiment, representative of three. **e**, Flow cytometric analysis of $S1P_1$ on splenic CD4$^+$ L-selectin^{high} T cells from the indicated mice after treatment with poly(I:C) (PIC) or PBS. Control antibody staining is shown shaded in grey. Data are representative of ten mice of each type analysed in six experiments.

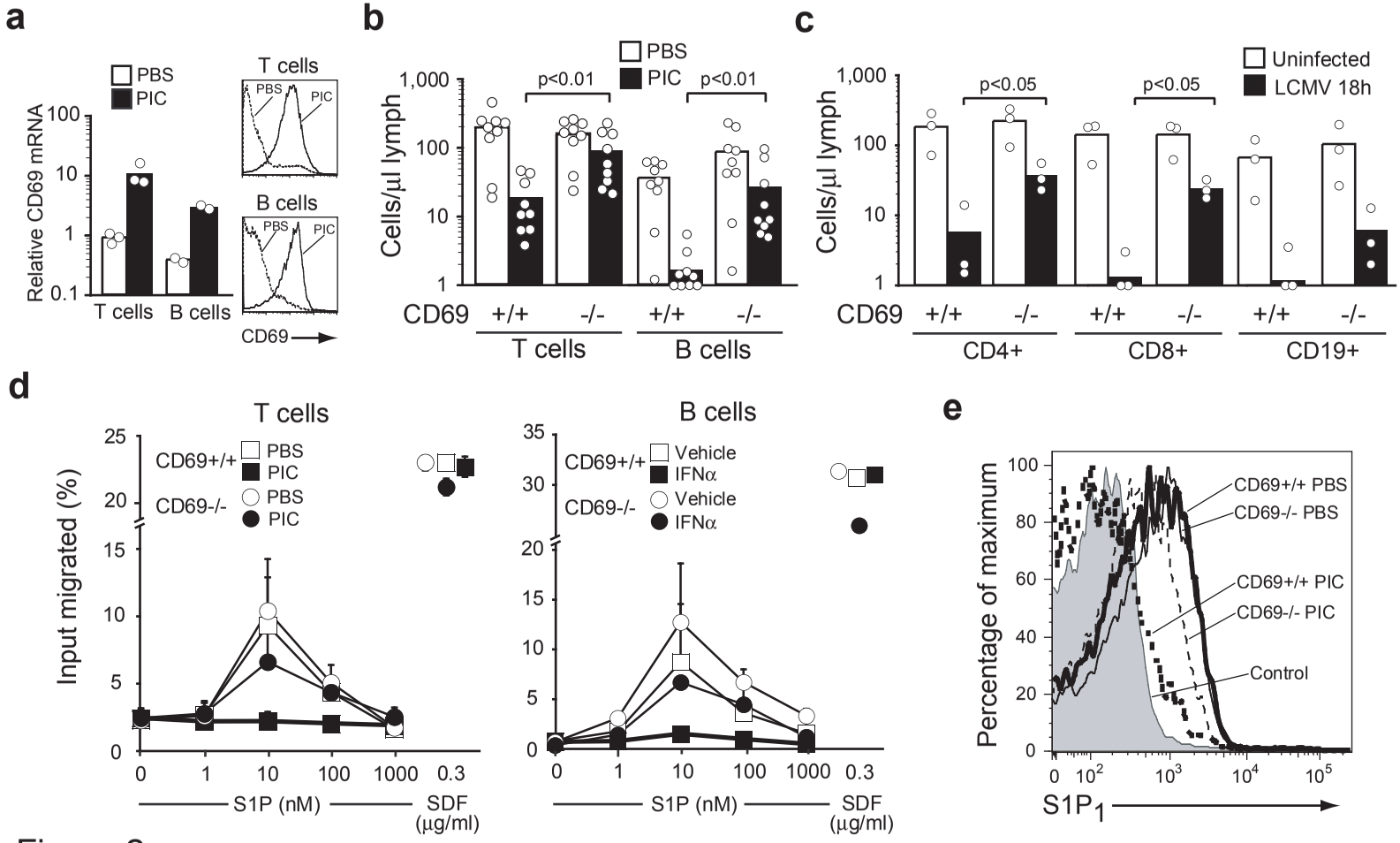
a
PBS
PIC
Relative CD69 mRNA
100
10
1
0.1
T cells
B cells
T cells
PBS
PIC
B cells
PBS
PIC
CD69
b
PBS
PIC
Cells/µl lymph
1,000
100
10
1
p<0.01
p<0.01
CD69
+/+
-/-
+/+
-/-
T cells
B cells
c
Uninfected
LCMV 18h
Cells/µl lymph
1,000
100
10
1
p<0.05
p<0.05
CD69
+/+
-/-
+/+
-/-
+/+
-/-
CD4+
CD8+
CD19+
d
T cells
CD69+/+
PBS
PIC
CD69-/-
PBS
PIC
Input migrated (%)
25
20
15
10
5
0
0
1
10
100
1000
0.3
S1P (nM)
SDF (µg/ml)
B cells
CD69+/+
Vehicle
IFNα
CD69-/-
Vehicle
IFNα
35
30
20
15
10
5
0
0
1
10
100
1000
0.3
S1P (nM)
SDF (µg/ml)
e
Percentage of maximum
100
80
60
40
20
0
CD69+/+ PBS
CD69-/- PBS
CD69+/+ PIC
CD69-/- PIC
Control
0
10²
10³
10⁴
10⁵
S1P1

Figure 2

Figure 3 | CD69 interacts with $S1P_1$ causing downregulation and inhibition of $S1P_1$ function. a, Diagram of retroviral constructs, and flow cytometric analysis of WEHI-231 cells transduced and stained to detect Flag-$S1P_1$, CD69 or hCD4, or showing GFP fluorescence as indicated. The plot of co-transduced cells shows the GFP^{high} gating strategy used in **b** and **c**. **b**, Flag-$S1P_1$ or Flag-$S1P_3$ expression in GFP^{high} $hCD4^+$ cells co-transduced with empty vector (EV), CD69 or CD23. The grey histogram shows staining of non-transduced WEHI-231 cells. Data are representative of three to six experiments. **c**, Migration assay of untransduced WEHI-231 cells (control; circles) and GFP^{high} $hCD4^+$ Flag-$S1P_1$ WEHI-231 cells co-transduced with EV (squares), CD69 (triangles) or CD23 (diamonds). Results are means±s.d. for three experiments. **d**, Quantitative PCR analysis of CD69 abundance in sorted B cells and mature CD4 single-positive (SP) L-$selectin^{high}$ thymocytes from mice reconstituted with wild-type (open columns) or $S1p_1^{-/-}$ (filled columns) fetal liver cells. Transcripts obtained from total brain are shown for comparison. **e**, Flag-$S1P_1$ and CD69 expression on total GFP^+ $hCD4^+$ Flag-$S1P_1$ WEHI-231 cells co-transduced with CD69. Inset: GFP levels of cells in regions 1 and 2. **f**, CD69 expression on GFP^{low} cells transduced with CD69 alone or co-transduced with Flag-$S1P_1$. The grey histogram shows staining of non-transduced WEHI-231 cells. **g**, Flag-$S1P_3$ and CD69 expression on Flag-$S1P_3$ WEHI-231 cells co-transduced with CD69. **h**, Flag-$S1P_1$ and CD69 expression on Flag-$S1P_1$ WEHI-231 cells co-transduced with CD69 and incubated for 6 h with 200 ng ml^{-1} pertussis toxin.

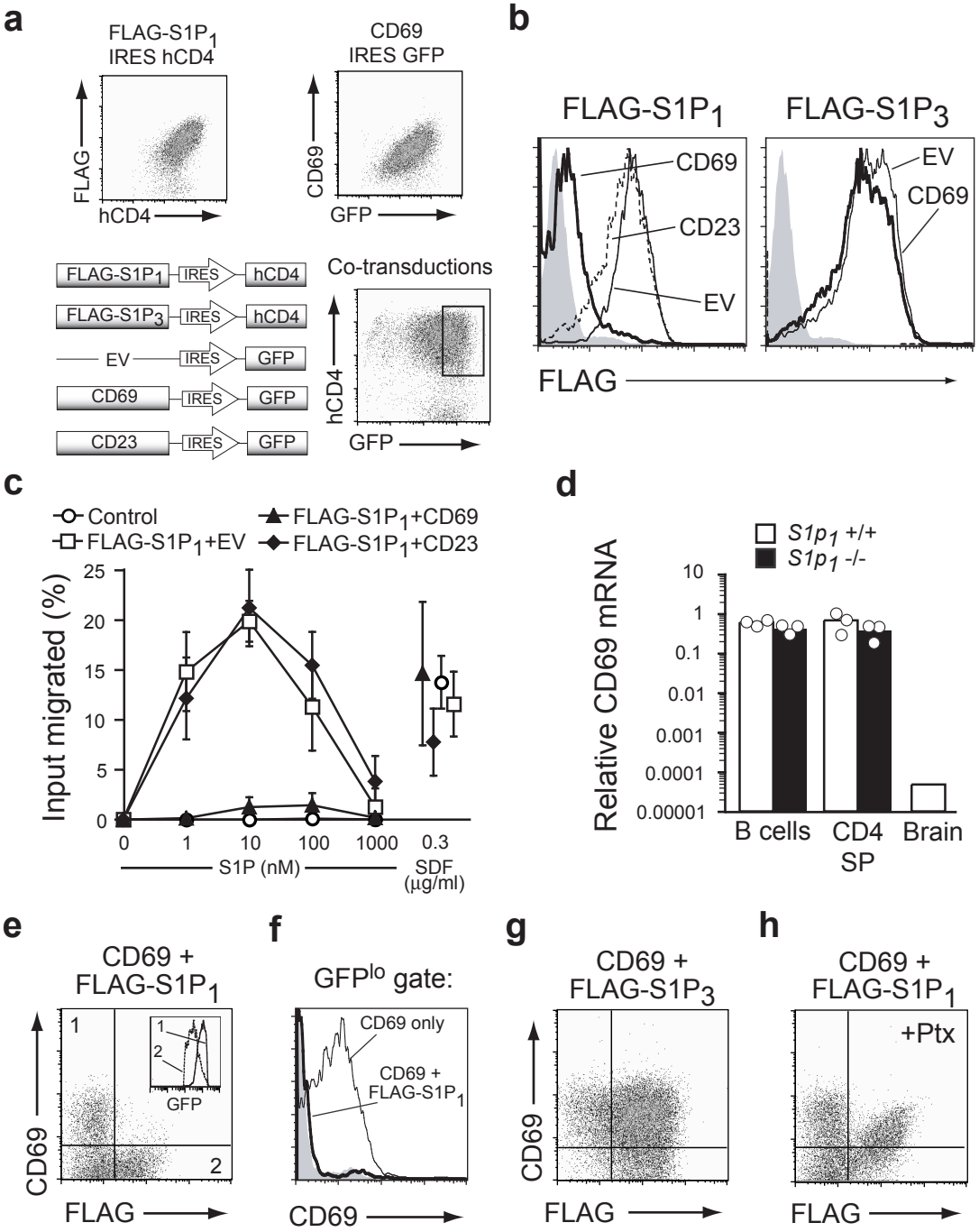
a
FLAG-S1P1
IRES hCD4
FLAG
hCD4
CD69
IRES GFP
CD69
GFP
FLAG-S1P1 IRES hCD4
FLAG-S1P3 IRES hCD4
EV IRES GFP
CD69 IRES GFP
CD23 IRES GFP
Co-transductions
hCD4
GFP
b
FLAG-S1P1
FLAG-S1P3
CD69
CD23
EV
EV
CD69
FLAG
c
Control
FLAG-S1P1+EV
FLAG-S1P1+CD69
FLAG-S1P1+CD23
Input migrated (%)
25
20
15
10
5
0
0
1
10
100
1000
0.3
S1P (nM)
SDF (μg/ml)
d
S1p1 +/+
S1p1 -/-
Relative CD69 mRNA
10
1
0.1
0.01
0.001
0.0001
0.00001
B cells
CD4 SP
Brain
e
CD69 + FLAG-S1P1
1
2
GFP
CD69
FLAG
f
GFPlo gate:
CD69 only
CD69 + FLAG-S1P1
CD69
g
CD69 + FLAG-S1P3
CD69
FLAG
h
CD69 + FLAG-S1P1
+Ptx
FLAG

Figure 3

Figure 4 | **Mouse and human CD69 interact with $S1P_1$. a**, 2B4 NFAT-GFP reporter cells were singly transduced or co-transduced as indicated. Receptors were crosslinked with plate-bound antibodies (open columns, isotype control; grey column, anti-CD69; black columns, anti-Flag) and the expression of GFP, shown as geometric mean fluorescence intensity (MFI), was analysed 16 h later. Data are shown as means±s.d. and are pooled from three experiments. **b**, Lysates of WEHI-231 cells transduced with the indicated retroviral constructs were immunoprecipitated (IP) with anti-Flag. Coimmunoprecipitated proteins were detected by using anti-haemagglutinin (anti-HA) or anti-Flag antibodies. Data shown are representative of four independent experiments. NS, non-specific band; WB, western blot. **c**, Lysates of Jurkat cells transfected with $S1P_1$-Myc or an empty vector and stimulated or not with anti-TCR antibody C305 to upregulate CD69 expression were immunoprecipitated with anti-CD69 or anti-Myc antibodies. Coimmunoprecipitated proteins were detected on western blots by using anti-CD69 and anti-Myc antibodies. Data shown are representative of three independent experiments. All markers are in kDa.

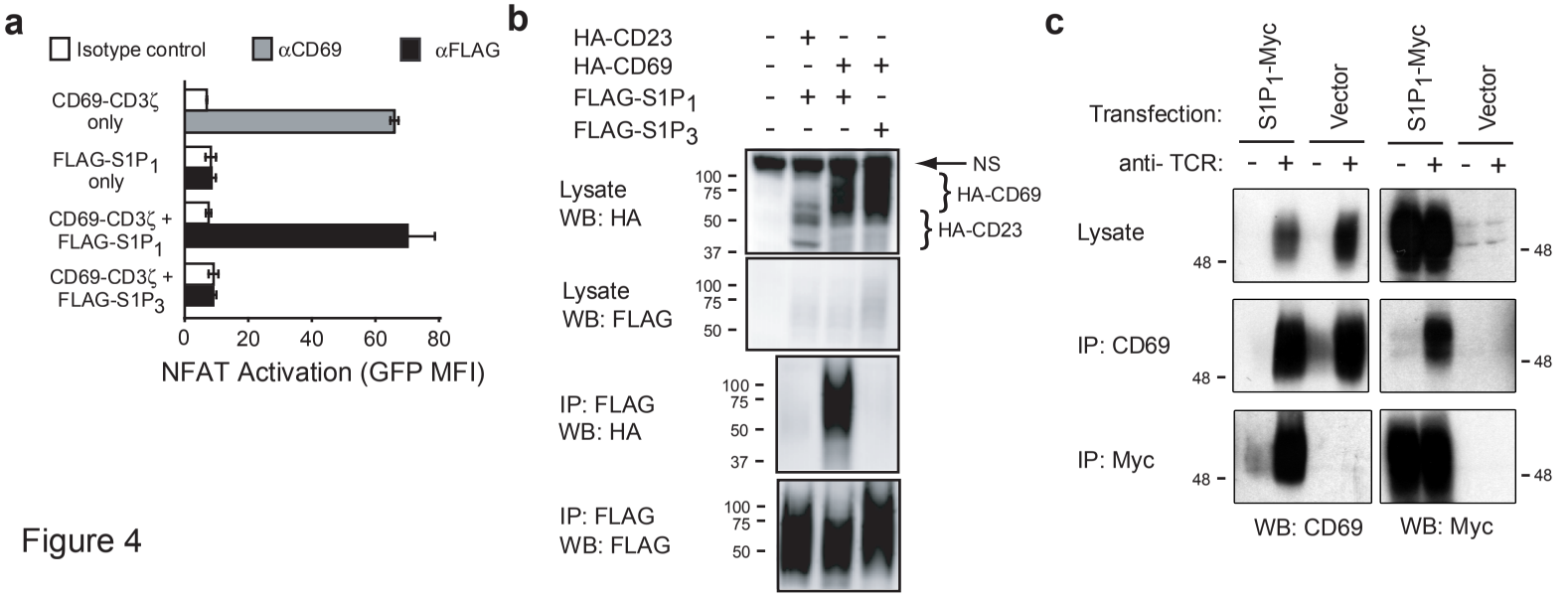
a
Isotype control
αCD69
αFLAG
CD69-CD3ζ only
FLAG-S1P1 only
CD69-CD3ζ + FLAG-S1P1
CD69-CD3ζ + FLAG-S1P3
0
20
40
60
80
NFAT Activation (GFP MFI)
b
HA-CD23
HA-CD69
FLAG-S1P1
FLAG-S1P3
Lysate WB: HA
Lysate WB: FLAG
IP: FLAG WB: HA
IP: FLAG WB: FLAG
100
75
50
37
NS
HA-CD69
HA-CD23
c
Transfection:
S1P1-Myc
Vector
anti- TCR:
Lysate
IP: CD69
IP: Myc
48
WB: CD69
WB: Myc

Figure 4

Supplementary Figure 1

Lymphocyte intrinsic IFNAR1 requirement during PolyI:C-induced lymphocyte sequestration **a,** Mice were injected with PBS or poly I:C and at the indicated times the number of each lymphocyte population in blood was determined. Points indicate mean (±sd) for three poly I:C-treated mice per time point. The "0" h data are from mice injected 6 h earlier with PBS. Data are from the same experiment shown in Figure 1a. **b,** Wild-type and IFNAR1-deficient lymphocytes were labeled with CFSE and CMTMR, respectively, transferred into wild-type mice and after 36 h, groups of three mice were injected with poly I:C (PIC). At 6 h after treatment blood was analyzed for the number of transferred cells. Bars represent averages of three mice per group and open circles represent individual animals. Data are from the same two experiments shown in Figure 1c and are representative of five. Two-tailed paired Student's t test was performed.

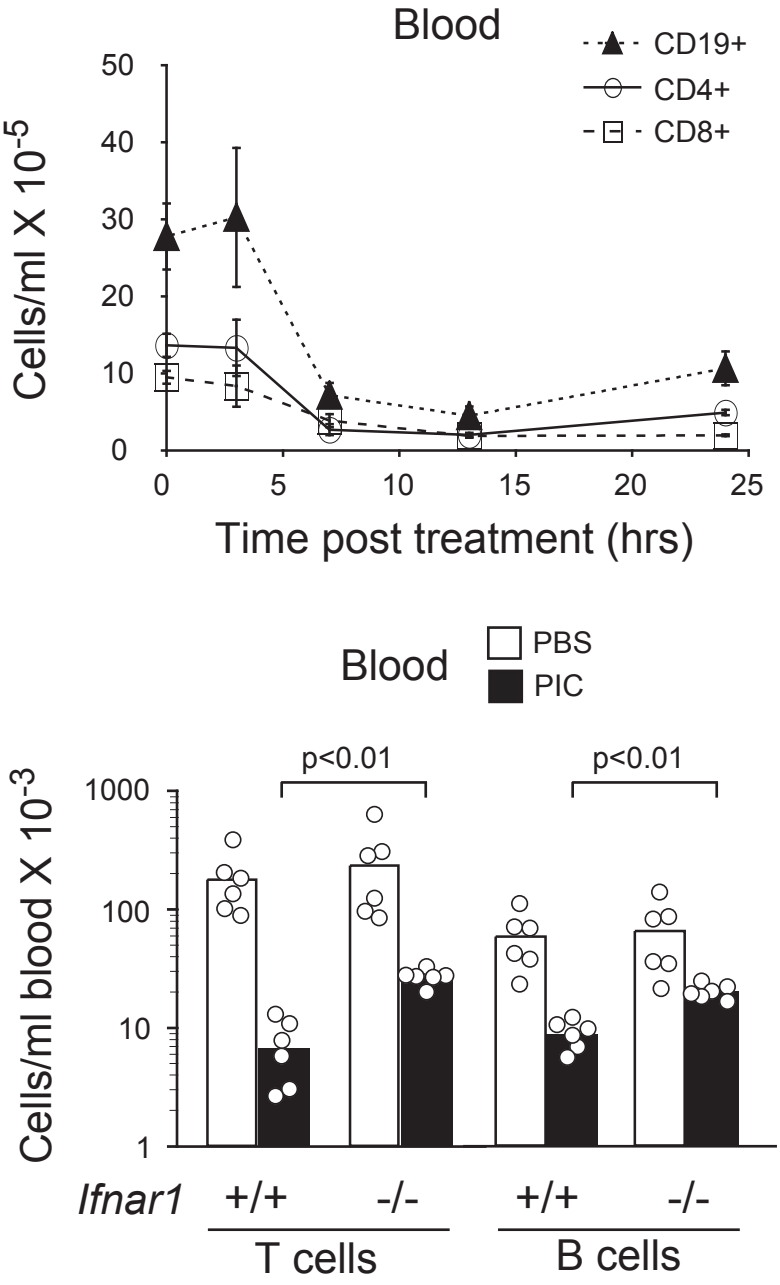

Suppl. Figure 1

Supplementary Figure 2

CD69-deficient cells are resistant to polyI:C-induced sequestration and regulate IRF7 and $S1P_1$ transcripts similarly to wild-type cells. **a,** Wild-type and CD69-deficient lymphocytes were labeled with CFSE and CMTMR, respectively, transferred into wild-type mice and after 36 h, groups of three mice were injected with poly I:C (PIC). At 6 h after treatment blood were analyzed for the number of transferred cells. Bars represent averages of three mice per group and open circles represent individual animals. Data are from the same three experiments shown in Figure 2b. Two-tailed paired Student's t test was performed. **b and c,** Quantitative PCR analysis of IRF7 (b) and $S1P_1$ (c) in sorted T cells and B cells from *CD69-/-* mice treated for 6 h with polyI:C or PBS, expressed as relative amount of the indicated messenger RNA normalized to HPRT.

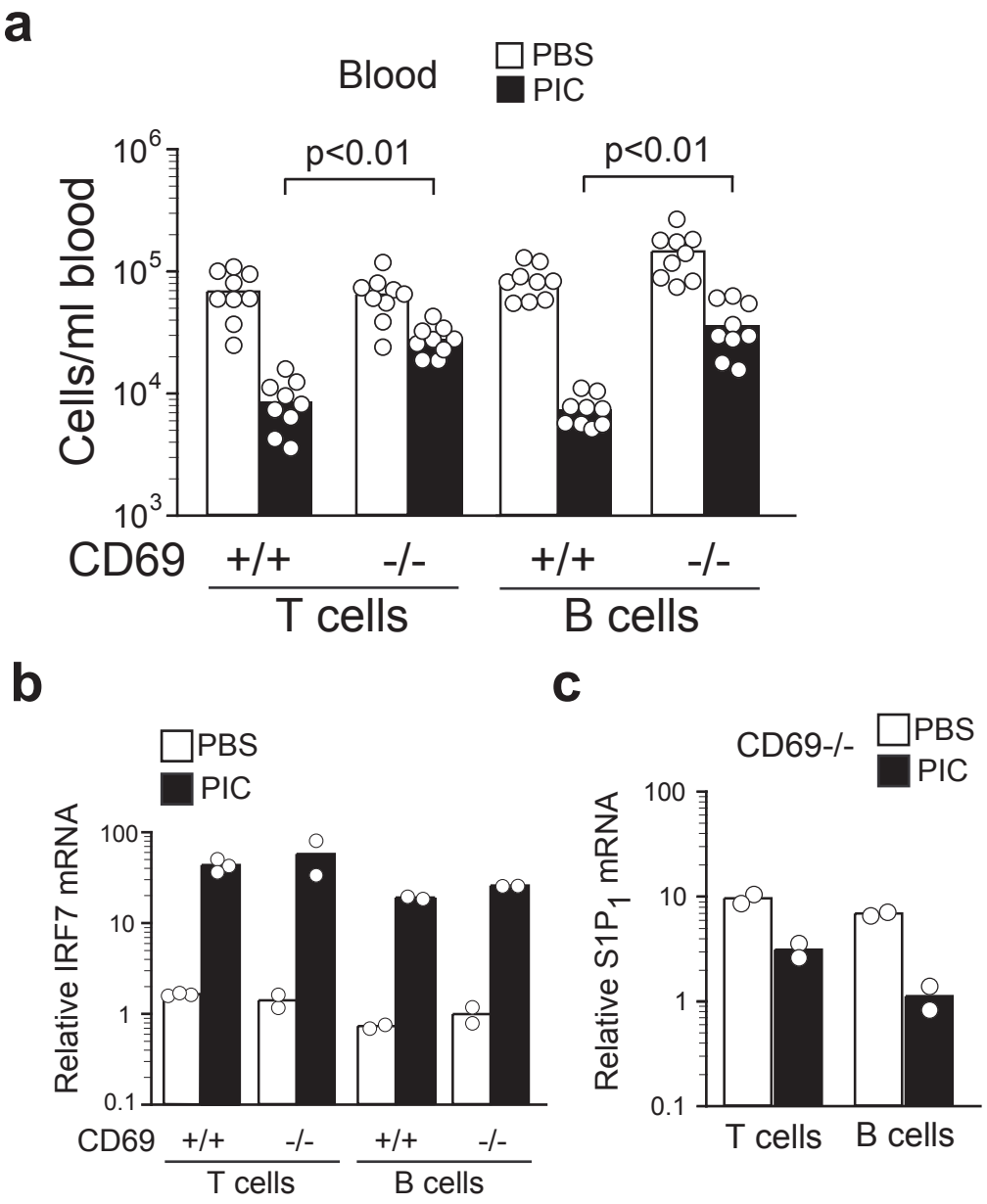

Suppl. Figure 2

Supplementary Figure 3

LCMV induced lymphocyte sequestration and $S1P_1$ down-regulation is CD69 dependent. **a,** Wild-type and CD69-deficient lymphocytes were labeled and transferred into wild-type recipient mice. Twenty-four hours post-transfer, mice were uninfected or infected with $2x10^6$ pfu Armstrong strain LCMV and analyzed at 18 h post-infection for cell numbers in blood. Bars represent means and open circles are individual mice. Statistical analysis was performed by a two-tailed paired Student's t test. Data shown are representative of three experiments and are from the same experiment shown in Figure 2c. **b,** Flow cytometric analysis of CD69 expression on uninfected (blue) or LCMV infected (red) wild-type lymphocyte subsets. Staining of *CD69-/-* cells is shown in shaded gray. **c,** Flow cytometric analysis of $S1P_1$ abundance on the surface of splenic $CD4^+$ L-$selectin^{hi}$ T cells from the wild-type (blue) and *CD69-/-* (red) mice uninfected (thick) or infected (thin) with LCMV. Control antibody staining in shaded gray. Data are representative of 9 mice of each type analyzed in 3 experiments. Wild-type and *CD69-/-* cells equally upregulated the activation marker Ly6C at 40 h (data not shown).

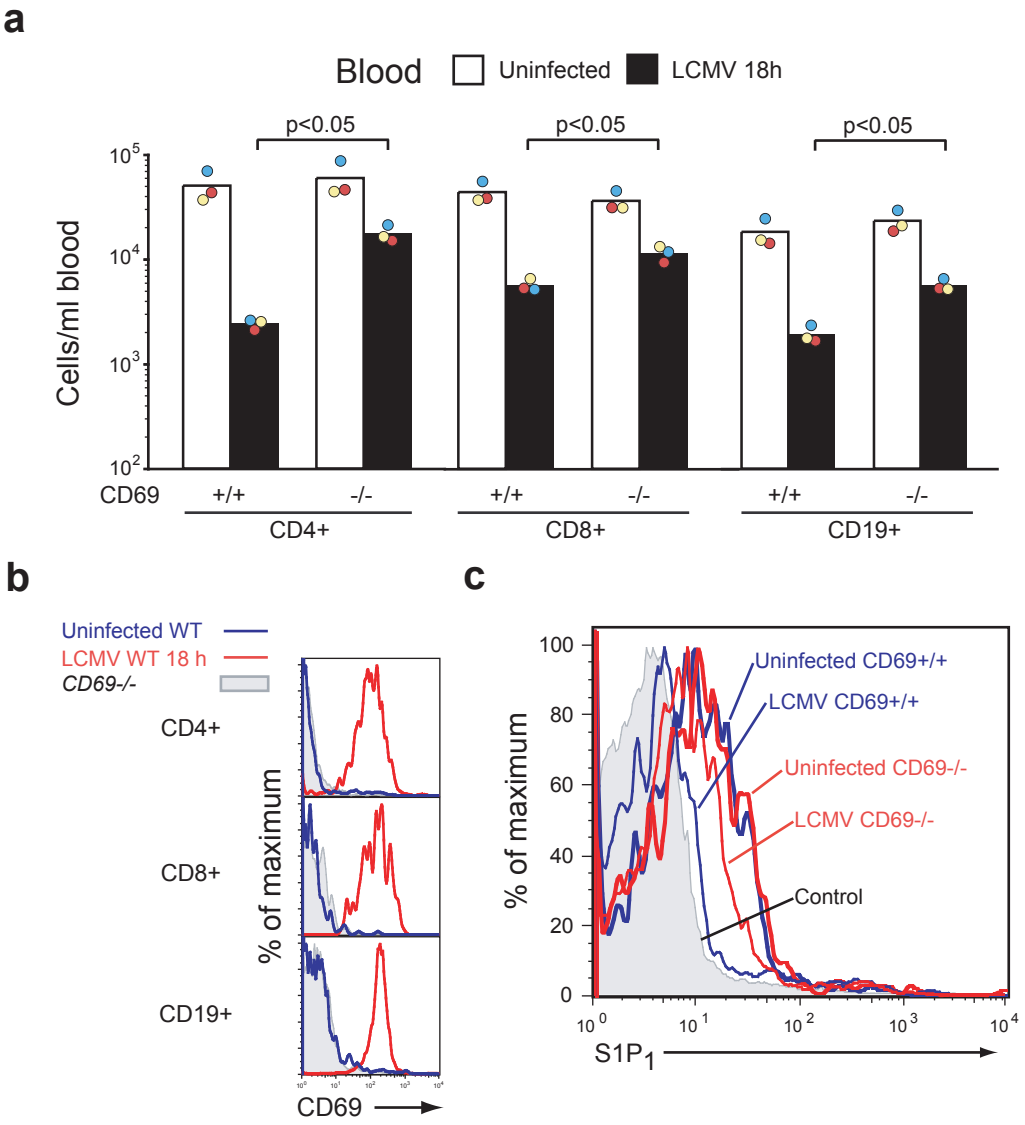

Suppl. Figure 3

Supplementary Figure 4

CD69-CD3z is coexpressed on the cell surface with $S1P_1$. **a and b,** Flow cytometric analysis of FLAG-$S1P_1$ and CD69-CD3z expression on 2B4 NFAT-GFP reporter cells (a) or WEHI231 cells (b). Cells were transduced with or without the indicated retroviral constructs. To generate 2B4 cells transduced with both constructs, cells that had been transduced with CD69-CD3z (a, upper right) were further transduced with FLAG-$S1P_1$ (a, lower right), To generate WEHI231 cells transduced with both constructs, cells that had been transduced with FLAG-$S1P_1$ (b, lower left) were further transduced with CD69-CD3z (b, lower right).

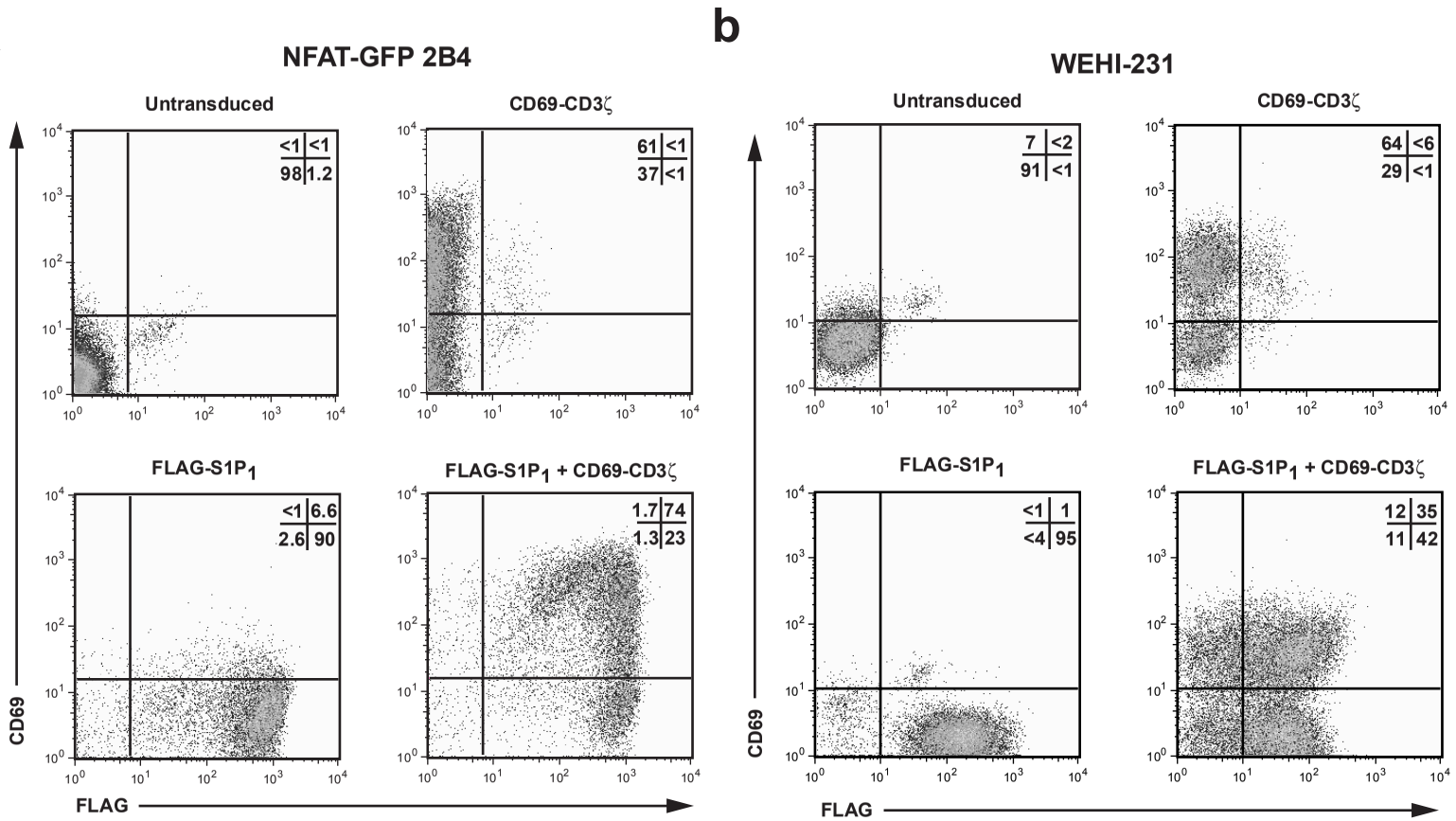

Suppl. Figure 4

CHAPTER 3

Coronin-1A is mutated in a thymic egress defective mouse strain and a T-B+NK+ SCID patient

Abstract

T cell exit from the thymus is necessary for adaptive immunity and is defective in mice carrying the recessive *ptcd* (peripheral T cell deficiency) locus. We find that *ptcd* T cells have an intrinsic migration defect, impaired lymphoid tissue trafficking, and irregularly shaped protrusions. The *ptcd* locus contains an E26K point mutation within the actin regulator Coronin-1A that enhances Arp2/3 inhibition in actin polymerization assays and mislocalizes the protein from the leading edge of migrating T cells. Discovery of a second Coronin-1A mutant during an ENU-mutagenesis screen for T-lymphopenic mice prompted us to identify an atypical human T-B+NK+ SCID patient with Coronin-1A deficiency. These findings add new insight to Arp2/3 regulation by Coronin-1A during T cell trafficking and demonstrate the utility of mouse forward genetics in identifying causes of rare human primary immunodeficiencies.

Introduction, Results and Discussion

Following development in the thymus, mature thymocytes upregulate sphingosine-1-phosphate receptor 1 ($S1P_1$) and exit into the circulation to populate the naïve T cell compartment. $S1P_1$ and its ligand sphingosine-1-phosphate (S1P) are required for egress of mature thymocytes (*1*). FTY720, a small molecule immunosuppressant in clinical trials for treatment of autoimmune disease, inhibits egress by modulating $S1P_1$ function (*1*). Beyond the $S1P_1$ requirement, little is understood about how T cells migrate out of the thymus. Initially isolated in the 1960's for exhibiting cataracts and microphthalmia (*2*), the Cataract Shionogi (CTS) mouse was later established to have a thymic egress defect (*3*) after CTS mice failed to reject MHC-disparate skin grafts (*4*). The nature of this recessive defect, named *ptcd* (peripheral T cell deficiency), and its role in thymic egress has been unclear.

To characterize the cellular basis for the *ptcd* defect, we first backcrossed the *ptcd* locus onto the C57BL/6 (B6) strain and confirmed the accumulation of mature single-positive (SP) thymocytes ($CD69^{lo}$ $CD62L^{hi}$) and associated decrease in circulating T cells (Fig. 1A). Irradiated wildtype mice that had been reconstituted with *ptcd* bone marrow cells also had an accumulation of mature thymocytes and low circulating T cells (Fig. 1B) whereas reciprocal bone marrow chimeras did not exhibit such defects (fig. S1). These results localized the *ptcd* defect to a hematopoeitic-derived cell and implicated impaired thymic egress of mature thymocytes as a pathogenic mechanism.

While normal amounts of $S1P_1$ were expressed on *ptcd* mature SP thymocytes (Fig. 1C), S1P1 function was impaired. In transwell migration assays, *ptcd* mature CD4SP thymocytes were less efficient at migrating towards S1P than cells from control heterozygous littermates (Fig 1D). The cells also migrated less efficiently to chemokines CCL21 and CXCL12. The response of *ptcd* CD4 and CD8 double positive (DP) thymocytes to CXCL12 was similarly reduced (Fig 1E) and migration of *ptcd* naïve splenic T cells was impaired while B cells migrated normally (Fig 1F). These results indicate that T cells in *ptcd* mice have a general, cell-intrinsic migration defect that impairs S1P1 responsiveness and blocks thymic egress.

To test for peripheral trafficking defects, *ptcd* and control T cells were co-transferred into wildtype recipients. At 1 h post-transfer, the ratio of *ptcd*:control T cells was decreased in peripheral and mesenteric lymph nodes and increased in blood (Fig 1G) indicating that *ptcd* cells are less efficient at entering lymph nodes. At 24 h after transfer a significantly reduced proportion of *ptcd* cells were found in lymph compared to lymph nodes (Fig. 1H). When entry into lymph nodes was blocked for 20 h with integrin-neutralizing antibodies, 60% of *ptcd* T cells were retained in the lymph nodes compared with just 20% of control T cells (Fig. 1I). These results demonstrate that *ptcd* T cells are defective in egressing from lymph nodes into lymph. Two-photon microscopy on explanted lymph nodes from mice that had received fluorescently labeled cells showed that while control cells moved at median velocities of 9.5 microns/min, *ptcd* cells moved at reduced median velocities of 6.6 microns/min (Fig. 1J and Movie S1). In addition,

ptcd cells had increased turning angles (Fig. 1K), indicative of less directed paths and the cells failed to efficiently displace over time (Fig. 1L). These results demonstrate that in addition to blocking thymic egress, the *ptcd* defect impairs trafficking through lymph nodes.

The *ptcd* locus was previously mapped to a 10.9 Mb region of chromosome 7 containing over 300 open reading frames (*5*). To refine the locus, a mapping cross was performed with B6. Using the thymic accumulation phenotype (Fig. 2A), we analyzed over 900 meiosis events and further mapped the *ptcd* locus to a 950 kb critical interval (Fig. 2B). This gene-rich interval contained 37 open reading frames including Coro1A (Fig. 2C). Coro1A was an attractive candidate gene for *ptcd* because of its abundance in T cells (*6*) and the association of coronin family molecules with actin-based motility (*7*). Sequencing of *ptcd* DNA revealed a G→A mutation in exon 2 of Coro1A (Fig. 2D), resulting in a non-conservative Glu→Lys substitution at residue 26 (E26K) in the beta-propeller domain (Fig. 2E). This residue is conserved in all annotated Coro1A sequences as well as charge conserved in a broad number of orthologs (fig. S2) and is in a surface exposed loop (*8*) adjacent to a region implicated in the close relative, Coro1B, as an actin binding site (*9*). Western blot analysis showed Coro1A abundance in total thymocytes did not vary between *ptcd* and controls (Fig. 2F).

In parallel to the above studies, we conducted an ethylnitrosourea (ENU)-mutagenesis screen to identify regulators of lymphocyte trafficking and egress.

Koyaanisqatsi (*koy*) was initially identified as a recessive mutant with a peripheral T cell deficiency (fig S3). Further characterization of *koy* mice revealed a decrease in mature thymocyte numbers (Fig. 2G). In transwell migration assays, *koy* thymocytes and naïve T cells migrated much less efficiently than littermate control cells (fig. S4). These findings in the *koy* mice, along with an elevated phalloidin staining in *koy* mature thymocytes (fig. S5), resembled those reported in Coro1A-/- mice generated by gene targeting (*10*). Upon sequencing *koy* DNA, we identified an A→T substitution in exon 7 of Coro1A (fig. S6) resulting in an Asp→Ala mutation at residue 278 (Fig. 2E). This residue is located at a contact surface predicted to be critical for the proper assembly and stability of Coro1A (*8*), and western blot analysis of total thymocytes showed that *koy* cells had roughly 10-fold reduced amounts of Coro1A (Fig. 2G). Taken together, these data indicate that *koy* is a hypomorphic mutant of Coro1A.

A direct comparison of *ptcd* with *koy* and Coro1A-/- mice confirmed that the E26K mutation does not phenocopy the Coro1A deficient state. While *ptcd* mutants have an accumulation of mature thymocytes (Fig. 1A), Coro1A-deficient mice have reduced numbers (Fig. 2H) due to reduced cell survival (*10*). Analysis of cell viability by loss of mitochondrial membrane potential (Fig. 3A) and annexin-V staining (Fig. 3B) revealed that mature thymocytes from *ptcd* mice were comparable to wildtype controls whereas mature thymocytes from Coro1A-/- mice had reduced viability. However, *ptcd* splenic T cells showed a similar defect in survival to Coro1A-/- cells (Fig. 3A, B). A previous study has attributed the survival defect of Coro1A-/- T cells to downstream effects of

excessive F-actin accumulation (*10*). Consistent with this interpretation, *ptcd* mature thymocytes showed only a minor increase in F-actin as measured by phalloidin staining (Fig. 3C) whereas Coro1A-/- mature thymocytes and the similarly apoptosis prone *ptcd* and Coro1A-/- splenic T cells all showed comparable two-fold elevations in phalloidin staining (Fig. 3C). A more recent study has suggested that the reduced viability of Coro1A-/- cells reflects a requirement for Coro1A in T cell receptor (TCR)-induced Ca^{2+} flux rather than in F-actin regulation (*11*). However, *ptcd* and Coro1A-deficient mature CD4 SP thymocytes showed comparable Ca^{2+} flux defects following CD3 crosslinking (Fig 3D), and minimal defects following co-crosslinking of CD3 and CD4 (Fig. 3D), dissociating the role of Coro1A in TCR-induced Ca^{2+} signaling from the defect in Coro1A-/- thymocyte viability.

Coro1B regulates F-actin dynamics at the leading edge of migrating fibroblasts (*12*) and in migrating wildtype T cells, Coro1A was situated in F-actin- and Arp2/3-rich leading edge protrusions (Fig. 3E and F). The distribution of $Coro1A^{E26K}$ in migrating *ptcd* T cells was markedly altered and little of the protein could be detected at the leading edge (Fig. 3E and F). Real-time live cell imaging revealed that protrusions from migrating *ptcd* T cells were irregularly shaped and often larger in size, consistent with a failure to properly regulate the actin cytoskeleton (Fig. 3G and Movies S2-4). The short *in vitro* survival of Coro1A-deficient T cells made assessments difficult, but these cells appeared more severely compromised in their migration than *ptcd* T cells (Movie S5).

To understand the biochemical impact of the E26K mutation, we first looked at Coro1A's ability to bind F-actin. Surprisingly, in co-sedimentation assays, Coro1A^{E26K} associated normally with F-actin (Fig. 3H). By contrast, Arp2/3 failed to efficiently immunoprecipitate with Coro1A^{E26K} (Fig. 3I). Despite the purified proteins also showing a weaker interaction (Fig. 3J), Coro1A^{E26K} was more efficient than wildtype Coro1A at inhibiting Arp2/3 activity (Fig. 3K). This result suggests that the ability of Coro1A to bind to the Arp2/3 complex does not strictly correlate with its ability to inhibit nucleation in this assay. To examine how this biochemical gain-of-function mutation manifests as a recessive *ptcd* allele, we analyzed T cells from ptcd/+ and ptcd/- mice. As expected, the Coro1A distribution in *ptcd/-* and ptcd/ptcd T cells was similar (Fig. 3L). In *ptcd/+* T cells, Coro1A was present both at and mislocalized away from the leading edge. These results suggest that in ptcd/+ heterozygote cells, Coro1A^{WT} can access the leading edge to regulate actin dynamics. Taken together, these data indicate that the Glu26 residue is critical for Coro1A localization and Arp2/3 regulation in T cells.

With Coro1A point mutations causing severe T lymphopenia in both *ptcd* and *koy*, we asked whether mutations in Coro1A could also be responsible for human primary T cell immunodeficiency cases with undefined etiologies. Thus, we sequenced DNA from sixteen T-B+NK+ SCID patients with unknown causes for mutations in *CORO1A* and identified a patient with a two nucleotide deletion in exon 3, c.248 249delCT (Fig. 4A), resulting in a frameshift and premature stop codon (p.Pro83ArgfsX10) within the Coro1A beta-propeller domain. Consistent with a destabilizing truncation, western blot analysis

of Epstein Barr virus-immortalized B lymphoid cell lines derived from the patient's peripheral blood showed an absence of Coro1A protein (Fig. 4B). When this patient was 1 yr old, she was hospitalized with a severe post-vaccination varicella infection and she was later diagnosed as an atypical T-B+NK+ SCID patient and treated by allogeneic bone marrow transplantation. The father was heterozygous for the *CORO1A* 2bp deletion (Fig. 4A), but it was not found in the patient's mother or sister. To test for *CORO1A* gene copy loss in the patient, we analyzed buccal genomic DNA on Affymetrix SNP 6.0 genechips. A segment containing Coro1A was deleted from ~29.5Mb to ~30.1Mb of chromosome 16 in the patient but not her mother (Fig. 4C). Deletion of this same segment has recently been linked to autism and various developmental defects (*12-15*). Thus, we identified two separate mutations resulting in Coro1A deficiency in a T-B+NK+ SCID patient: an inherited 2bp deletion and a de novo ~600kb microdeletion.

In summary, we establish that Coro1A is necessary for thymic and lymph node egress of T cells, adding this protein to the small number of other molecules known to be required for this process. Lymphocyte protrusions initiate diapedesis (*16*) and Coro1A-dependent actin control of thymocyte protrusions may play a critical role in T cell locomotion and thymic egress. Studies of Crn1, the yeast coronin homolog, proposed that Crn1 inhibits Arp2/3 through direct interaction and stabilization of an inactive Arp2/3 state (*17, 18*). Our findings with Coro1A^{E26K} are inconsistent with this model since this mutant shows reduced binding to the Arp2/3 complex, but increased ability to inhibit Arp2/3-induced nucleation *in vitro*. Future studies will be required to clarify the

mechanistic basis of Coro1A^{E26K} function and relate this function to phenotypes observed in the *ptcd* mice. The similar partial deficiencies in TCR-induced Ca^{2+} flux in Coro1A^{E26K} and Coro1A-/- cells add to mounting evidence that an intact actin cytoskeleton is important for TCR-induced Ca^{2+} flux (*19*). While the human X-linked Wiskott Aldrich syndrome has long associated actin biology with haematopoietic cell dysfunction, a mouse forward genetics approach has now allowed us to link Coro1A regulation of actin cytoskeleton with T-B+NK+ SCID, previously defined by mutations impairing antigen or cytokine receptor signaling (*20, 21*). A recent report classifying a Coro1A-null allele as an autoimmune-suppressing locus in mice (*22*) is consistent with Coro1A defects causing immunodeficiency. Because the pericentromeric segment of human chromosome 16 containing Coro1A is prone to copy number variation, we anticipate that additional T-B+NK+ SCID cases will involve Coro1A mutations.

Methods

Mice, ENU-mutagenesis, and bone marrow chimeras

C56BL/6 (B6) and B6-CD45.1 mice were obtained from Jackson Laboratories, National Cancer Institute, or a colony maintained at the University of California, San Francisco. UBC-GFP mice were purchased from Jackson Laboratories. Cataract Shionogi (CTS/Shi) mice were purchased from TGC (Tokyo, Japan). The *ptcd* locus was backcrossed 6-10 generations onto B6 using SNP markers as described below. Coro1A-/- mice, which were backcrossed 10 generations with B6, were generated as described (*10*). Koyaanisqatsi (*koy*) mice were identified in an ENU-mutagenesis screen performed as described (*23*) using B6 mice in a colony maintained at the Australian National University. Briefly, male B6 mice were treated with three doses, 1 wk apart, of 100 mg/kg N-ethyl-N-nitrosourea (Sigma) in 10% ethanol, citrate buffer (pH 5.0) to produce G0 mice. Following an 8 wk refractory period, these G0 males were mated with B6 females to generate G1 offspring. Two unrelated G1 mice were crossed producing G2 mice, which, were then intercrossed to yield G3 mice. Screening of these G3 mice by FACS identified the *koy* phenotype. All mice were housed in specific pathogen-free conditions; and all protocols were approved by the Institutional Animal Care and Use Committee of the University of California, San Francisco, or the Australian National University AEEC. Bone marrow chimeras were generated with 2-3 x 10^6 bone marrow cells from donor mice intravenously transplanted into lethally irradiated congenic hosts. Chimeras were given antibiotic water prophylacticly and analyzed 8-12 weeks after transplantation.

Flow cytometry, intracellular stains, and calcium flux measurements

S1P1 polyclonal antibody was previously described (*24*). Phalloidin-FITC was from Sigma. Indo-1 was from Invitrogen. Intracellular staining and Annexin-V staining kits were from BD Bioscience. JC-1 mitochondrial membrane potential staining kit was from Cayman Inc. All other antibodies used for flow cytometry were obtained from BD Biosciences, Invitrogen, eBiosciences, or BioLegend. Calcium flux assays were adapted from previously described methods for thymocytes (*25*). Briefly, cells were loaded at 30˚C for 30 min with Indo-1 in the presence of biotinylated anti-CD3 (clone 2C11, BD), anti-CD8 FITC (clone 53-6.7, BD), and anti-CD4 Alexa647 (clone RM4-5, BD). Thymocytes were additionally stained with anti-CD62L PE (clone Mel14, BD) and splenocytes with anti-CD44 PE (clone IM7, BD). Cells were washed and kept on ice until analysis. For anti-CD4 co-crosslinking, cells were additionally pre-treated for 5 min with biotinylated anti-CD4 (clone RM4-4, BD). Cells were mixed with pre-warmed media containing propidium iodide for exclusion of dead cells and warmed to 37˚C. Baseline calcium levels (ratio of UV-short to long) was assessed for 30 sec prior to streptavidin (50 ug/mL; Pierce) crosslinking. All flow cytometry was performed on BD FACalibur or BD LSRII.

Purification of Recombinant Protein

Coronin recombinant protein was expressed and purified with a mammalian expression system as described previously for Coronin 1B (*12*). Purified protein was quantified from absorbance at 280 nm and the predicted extinction coefficients of 62910 $M^{-1}cm^{-1}$ (Coronin 1A) and 65890 $M^{-1}cm^{-1}$ (Coronin 1B).

Immunoprecipitation

Cells were washed twice with phosphate-buffered saline and lysed with a KCl buffer (20 mM HEPES, pH 7.0, 100 mM KCl, 0.5% Nonidet P-40, 1 mM EDTA, 1 mM phenylmethylsulfonyl fluoride, 10 µg/ml 1,10-phenanthroline, 10 µg/ml aprotinin, 10 µg/ml leupeptin, 10 mM sodium fluoride, and 2 mM sodium orthovanadate). Lysates were cleared at 13,000 x *g* for 5 min and incubated with 0.5 µg of primary antibody for 16 h at 4 °C, followed by the addition of 20 µl of 50% slurry of ImmunoPure-immobilized protein A/G beads (Pierce) and further incubation at 4 °C for an additional hour. The immune complexes were collected, washed with the KCl buffer three times, separated by SDS-PAGE, and transferred to a polyvinylidene difluoride membrane (Bio-Rad) for Western blotting.

Direct Interaction Detection

StrepTactin Beads were saturated with 1% BSA in a KCl buffer (20 mM HEPES, pH 7.0, 100 mM KCl, 0.5% Nonidet P-40, 1 mM EDTA) by overnight incubation to block nonspecific binding. Each purified recombinant Coronin was added in excess to a 20 µL bed volume of the blocked StrepTactin Beads and incubated at 4°C for 1 hour. Purified Arp2/3 complex was added to a 50 nM concentration in a total volume of 200 µL of the KCl buffer and incubated for 1 hour at 4°C. Beads were subsequently washed three times with KCl buffer and resuspended in 2X SDS PAGE sample buffer for Western analysis.

Actin Assembly Assay

VCA-induced Arp2/3 nucleation reactions were performed as previously (*12*): recombinant Coronin and Arp2/3 (20 nM) were mixed in MKEI-50 Buffer and incubated at room temperature for 5 min; reactions were initiated by the simultaneous addition of 1.5 μM actin (5% pyrene labeled, primed with 1 mM EGTA and 0.1 mM $MgCl_2$ for 90 s) and 1 nM GST-VCA. The delay between mixing reactants and recording fluorescence was 15 seconds. Fluorescence was converted to the molar concentration of F-actin from the fluorescence of completely polymerized (24 hr post reaction) and unpolymerized actin, assuming a critical concentration of 0.1 μM.

Western Blot

Lysates from mouse thymocytes and human EBV-immortalized cell lines were prepared in RIPA buffer (1% NP-40, 0.5% sodium deoxycholate, 0.1% SDS, 50mM Tris-pH8.0, 150mM NaCl, 0.02 NaN3), resolved (NuPage, Invitrogen) and transferred (XCell, Invitrogen) to Immobilon-FL (Millipore), blocked and probed with LICOR buffer, and analyzed on an Odyssey Infrared Imager (LICOR). Anti-Coro1A from Upstate. Anti-actin from Sigma. Secondary IREDye antibodies from Rockland.

Transwell migration

Transwell migration assays (5 micron; Corning) were performed with thymocytes or splenocytes collected in migration media (RPMI (Cellgro) supplemented with 10 mM HEPES (Cellgro), 100 U/mL Penicillin/Streptomycin (Cellgro), and 0.5% Fatty Acid Free BSA (Calbiochem)). For S1P migration, thymocytes were assayed immediately after isolation. For chemokine migration, thymocytes or RBC-lysed splenocytes were resensitized in migration media for 30 min at 37˚C. S1P (Sigma), human SDF-1a

(Peprotech) and mouse CCL21 and CXCL13 (R&D Systems) were used at the concentrations indicated.

Adoptive cell transfers and treatments

Thymocytes were labeled with CFSE or CellTracker Orange CMTMR (Molecular Probes) as described (*26*). For adoptive transfer, mice were injected intravenously with ~1-3 x 10^7 cells in ~0.3 mL of media. For homing assays, mice were analyzed 1 h post-transfer. For peripheral egress assays, mice were analyzed 24 h post-transfer or treated intravenously with entry blocking antibodies for 20 h and analyzed after 44 h. Antibodies used for in vivo entry blockade were previously described (*27*).

Two-photon microscopy

Thymocytes from donor mice were isolated and labeled with CellTracker Orange CMTMR (Invitrogen-Molecular Probes) as described (*28*) and intravenously injected with thymocytes from UBC-GFP mice into B6 recipient mice. After 12-24 h, inguinal lymph nodes were isolated for two-photon microscopy, and axillary and brachial lymph nodes were isolated for flow cytometry. Flow cytometric analysis confirmed that >90% of CMTMR-positive cells in lymph nodes were mature single-positive thymocytes (CD4+CD8-CD69^{lo}CD62L^{hi} or CD4-CD8+ CD69^{lo}CD62L^{hi}). Explants were prepared as described (*29*). Inguinal lymph nodes were perfused with RPMI (Cellgro) at 36-37°C, aerated with 95% O_2/5% CO_2, and were imaged from the cortical side of the lymph node through the capsule. A 'custom' two-photon microscope system was used for imaging, with the 5-W MaiTai TiSapphire laser (Spectra-Physics) tuned at an 890 nm excitation wavelength. Images were captured with Video Savant software (IO Industries). For

time-lapsed imaging, 30-36 planes spaced 3 um apart were collected every 20 s. Each xy plane spanned 240 um x 288 um at a resolution 0.6 um per pixel. Data were further processed with MetaMorph software (Molecular Devices). Imaris software (Bitplane AG) was used for three-dimensional volume rendering and cell tracking. Matlab software was further used to calculate cell velocities, turning angles, and displacement. Statistical significance was evaluated with a paired two-tailed Student's t-test.

Genetic mapping, SNP analysis, and sequencing

CTS/Shi mice were crossed with B6 to generate an F1 generation. The *ptcd* locus was mapped with mutant F2 progeny from F1 intercrosses, F1 backcrossed to nonparental CTS, or mutant F2 crossed with nonparental F1. Mice were phenotyped by flow cytometric analysis of thymocyte subset frequencies. Genomic DNA was isolated from tails (Wizard Genomic Kit, Promega) and SNP reactions were performed with Amplifluor HT-kit (Chemicon/Millipore) on an ABI7300 (Applied Biosystems) according to manufacturer's instructions. Mapping SNPs were selected based on polymorphisms between B6 and BUB/J, a strain closely related to CTS/Shi. SNP primers were designed on the AssayArchitect website. Human genomic DNA was isolated from buccal swabs or EBV-immortalized lines with a Puregene kit (Gentra Systems, Minneapolis, MN). Genomic QPCR was performed on ABI7300. Human and mouse Coro1A exons and surrounding splice regions were amplified by PCR from genomic DNA, resequenced, and analyzed on 4Peaks relative to reference human genomic and cDNA sequences NM_007074 and NM_007074.2, respectively. Primers summarized in Supplemetary Table 1.

Brightfield and immunofluorescenct microscopy

For fixed immunofluorescent imaging, 1-2x10^6 lymphocytes from peripheral and mesenteric lymph nodes were seeded on chambered coverslips (Lab-tek, Nunc) precoated with 10 ug/mL recombinant mouse ICAM1-Fc (R&D Systems), and allowed to settle and migrate in the presence of 1 ug/mL CCL21 (R&D Systems) for 1 h at 37°C in RPMI (Cellgro) supplemented with 1% Fetal Calf Serum (Invitrogen), 10mM HEPES (Cellgro), and 100 U/mL Penicillin/Streptomycin (Cellgro). Cells were then fixed with 4% (wt/vol) paraformaldehyde (Sigma) and permeabilized with 0.5% Triton-X100 (Sigma) in PBS. Coverslips were then stained with a combination of the following: anti-Coronin-1A or anti-p34Arc (Upstate), FITC-conjugated phalloidin (Sigma), Alexa647-conjugated anti-CD4 (BD), Alexa647-conjugated anti-CD8 (BD), biotinylated goat anti-rabbit (BD), streptavidin-Cy3 (Jackson Immuno), or DAPI (Molecular Probes). Z-stacks were captured on an Axiovert Z1 (Zeiss) and deconvoluted with Axiovision Software (Zeiss). For real-time imaging, 5 x 10^5 lymphocytes from peripheral and mesenteric lymph nodes were stained with PE-conjugated anti-CD19 (BD) and Alexa647-conjugated anti-CD4 and anti-CD8 (BD) and seeded on ICAM-coated chambered coverslips with CCL21 as described above with the addition of 0.1% NuSieve GTG Low Melt Agarose (FMC BioProducts) and DAPI. Cells were maintained at 37˚C and 5% CO2 during 3-4 h of imaging in an environmentally-controlled stage on an Axiovert Z1. Each 5 min movie was generated with 10 s time-lapse intervals containing 6 brightfield 0.5 micron z-stacks. Following time-lapse, a fluorescence image was captured to identify live T cells. Movies

and images were processed with Axiovision (Zeiss) and exported for annotation and splicing with AfterEffects (Adobe).

Acknowledgements

We'd like to thank the patient and her family. We also thank M. Anderson, P. Beemiller, S. Cheung, G. Cinamon, M. Krummel, T. Phan, H. Phee, and A. Weiss for helpful discussions and D. Schafer for helpful advice and reagents related to the pyrene actin assay. This work was supported by the UCSF Medical Scientist Training Program and a Genentech-Sandler Graduate Research Fellowship (L.R.S.), the US Immunodeficiency Network and Jeffrey Modell Foundation (J.M.P.), the Howard Hughes Medical Institute (J.G.C.), and grants from the National Institutes of Health (C.C.G., J.B. and J.G.C.).

References

1. S. R. Schwab, J. G. Cyster, *Nature Immunology* **8**, 1295 (Dec, 2007).
2. H. Ohtori, T. Yoshida, T. Inuta, *Exp. Animals* **17**, 91 (1968).
3. H. Yagi *et al.*, *Journal of Immunology* **157**, 3412 (Oct 15, 1996).
4. S. Makino, Y. Muraoka, M. Harada, Y. Kishimoto, T. Konishi, in *Diabetes 1988: proceedings of the 13th Congress of the Interntaional Diabetes Federation* R. G. Larkins, P. Z. Zimmet, D. J. Chisholm, Eds. (Elsevier Science Pub. Co., Amsterdam, 1988) pp. 747-750.
5. S. Kimura *et al.*, *Immunogenetics* **47**, 278 (1998).
6. B. Nal *et al.*, *International Immunology* **16**, 231 (Feb, 2004).
7. A. C. Uetrecht, J. E. Bear, *Trends in Cell Biology* **16**, 421 (Aug, 2006).
8. B. A. Appleton, P. Wu, C. Wiesmann, *Structure* **14**, 87 (Jan, 2006).
9. L. Cai, A. M. Makhov, J. E. Bear, *Journal of Cell Science* **120**, 1779 (May 15, 2007).
10. N. Foger, L. Rangell, D. M. Danilenko, A. C. Chan, *Science* **313**, 839 (Aug 11, 2006).
11. P. Mueller *et al.*, *Nature Immunology* **9**, 424 (Apr, 2008).
12. L. Cai, T. W. Marshall, A. C. Uetrecht, D. A. Schafer, J. E. Bear, *Cell* **128**, 915 (Mar 9, 2007).
13. N. Ghebranious, P. F. Giampietro, F. P. Wesbrook, S. H. Rezkalla, *American Journal of Medical Genetics. Part A* **143**, 1462 (Jul 1, 2007).
14. R. A. Kumar *et al.*, *Human Molecular Genetics* **17**, 628 (Feb 15, 2008).

15. L. A. Weiss *et al.*, *New England Journal of Medicine* **358**, 667 (Feb 14, 2008).

16. C. V. Carman *et al.*, *Immunity* **26**, 784 (Jun, 2007).

17. C. L. Humphries *et al.*, *Journal of Cell Biology* **159**, 993 (Dec 23, 2002).

18. A. A. Rodal *et al.*, *Nature Structural and Molecular Biology* **12**, 26 (Jan, 2005).

19. E. M. Gallo, K. Cante-Barrett, G. R. Crabtree, *Nature Immunology* **7**, 25 (Jan, 2006).

20. J. M. Puck, F. Candotti, *New England Journal of Medicine* **355**, 1759 (Oct 26, 2006).

21. A. Fischer, *Immunity* **27**, 835 (Dec, 2007).

22. M. K. Haraldsson *et al.*, *Immunity* **28**, 40 (Jan, 2008).

23. K. A. Nelms, C. C. Goodnow, *Immunity* **15**, 409 (Sep, 2001).

24. C. G. Lo, Y. Xu, R. L. Proia, J. G. Cyster, *Journal of Experimental Medicine* **201**, 291 (Jan 17, 2005).

25. J. S. Maltzman, L. Kovoor, J. L. Clements, G. A. Koretzky, *Journal of Experimental Medicine* **202**, 893 (Oct 3, 2005).

26. L. R. Shiow *et al.*, *Nature* **440**, 540 (Mar 23, 2006).

27. T. H. Pham, T. Okada, M. Matloubian, C. G. Lo, J. G. Cyster, *Immunity* **28**, 122 (Jan, 2008).

28. C. D. Allen, T. Okada, H. L. Tang, J. G. Cyster, *Science* **315**, 528 (Jan 26, 2007).

29. T. Okada *et al.*, *PLoS Biology* **3**, e150 (May 3, 2005).

Figure 1. Peripheral T cell deficiency (*ptcd*) is an intrinsic T cell migration defect that impairs thymic egress and trafficking through lymph nodes. (**A and B**) Thymocyte and peripheral blood lymphocyte subsets from (A) B6 *ptcd* (white) and control mice (black) or (B) wildtype mice reconstituted with *ptcd* (white) or control (black) bone marrow. Columns represent means and circles represent individual mice. (**C**) Flow cytometric analysis of S1P1 on mature CD4SP thymocytes from *ptcd* (solid) and control (dotted) mice. Isotype control in filled histogram. **(D to F)** Transwell migration of *ptcd* (white) or control (black) mature CD4SP thymocytes to S1P in (D), thymocytes to indicated chemokines in (E), or splenic naïve CD4+ T cell or CD19+ B cells to indicated chemokines in (F), are shown as percentage of input that migrated. Columns represent means and circles represent individual mice pooled from three or four experiments. **(G)** Homing to lymph nodes 1 h following adoptive co-transfer of *ptcd* and control thymocytes. Ratio of *ptcd:*control normalized to injection ratio. Columns represent means and circles represent individual mice pooled from three experiments. **(H)** Ratio of *ptcd:*control cells in lymph and lymph nodes 24 h following adoptive transfer. Columns represent means and circles represent individual mice pooled from three experiments. **(I)** Lymph node retention of *ptcd* or control cells 20 h following entry blockade. Columns represent means and circles represent average values from independent experiments conducted with four mice each. **(J to L)** Time-lapse two-photon microscopy of explanted lymph nodes containing *ptcd* and heterozygote control cells. Data representative of three independent experiments with at least 40 tracks analyzed in each. Mean velocities (J) and turning angles (K) of *ptcd* cells (white) or

control cells (black). Columns represent means and circles represent individual experiments. (L) Average of displacement squared $<R^2>$ over time of *ptcd* (open diamond) or control cells (black circle). Symbols represent means and bars represent standard deviation. ** p-value<0.5

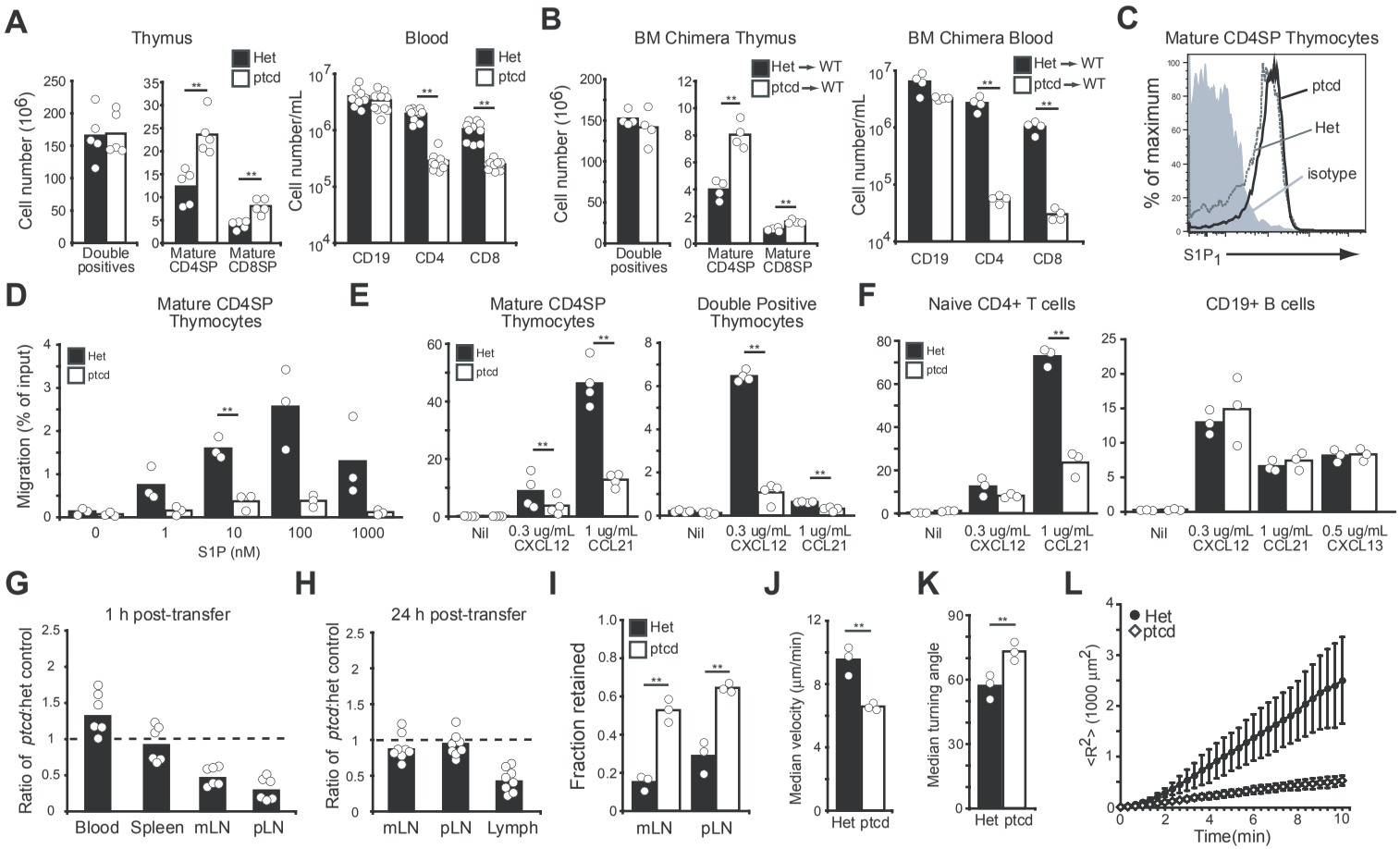
A
Thymus
Blood
Het
ptcd
Cell number (10^6)
Cell number/mL
Double positives
Mature CD4SP
Mature CD8SP
CD19
CD4
CD8
B
BM Chimera Thymus
BM Chimera Blood
Het → WT
ptcd → WT
C
Mature CD4SP Thymocytes
% of maximum
ptcd
Het
isotype
S1P1
D
Mature CD4SP Thymocytes
Migration (% of input)
S1P (nM)
E
Mature CD4SP Thymocytes
Double Positive Thymocytes
Nil
0.3 ug/mL CXCL12
1 ug/mL CCL21
F
Naive CD4+ T cells
CD19+ B cells
0.5 ug/mL CXCL13
G
1 h post-transfer
Ratio of ptcd:het control
Blood
Spleen
mLN
pLN
H
24 h post-transfer
Lymph
I
Fraction retained
J
Median velocity (μm/min)
K
Median turning angle
L
<R2> (1000 μm2)
Time(min)

Figure 1

Figure 2. *ptcd* and ENU-mutant *koy* are mutated in Coro1A

(A) Representative flow cytometric analysis of *ptcd* mapping cross progeny used to phenotype affected or unaffected mice. Phenotype scored on single-positive frequencies, fraction of $CD62L^{hi}$ $CD69^{lo}$ CD4SP, and expression level of CD62L in CD8SP. **(B)** *ptcd* critical interval defined by SNP markers polymorphic between B6 (black) and CTS (white) within indicated recombinant mice. **(C)** Schematic of open reading frames within the 950kb *ptcd* critical interval (adapted from Ensembl). **(D)** Dideoxy sequence tracings of DNA from *ptcd* and heterozygous mice revealing a 76G→A mutation causing a protein E26K substitution. DNA from the related NOD mouse strain was used as an additional control. **(E)** Schematic of Coro1A structure with *ptcd* and *koy* point mutations indicated. **(F)** Western blot analysis of total thymocytes from *ptcd* and control mice for Coro1A and actin. Samples loaded in three-fold dilutions. NC, negative control (Coro1A-/-). **(G)** Thymocyte subsets from *koy* (white) and control (black). Columns represent means and circles represent individual mice. **(H)** Western blot analysis from *koy* and control mice as described in (F).

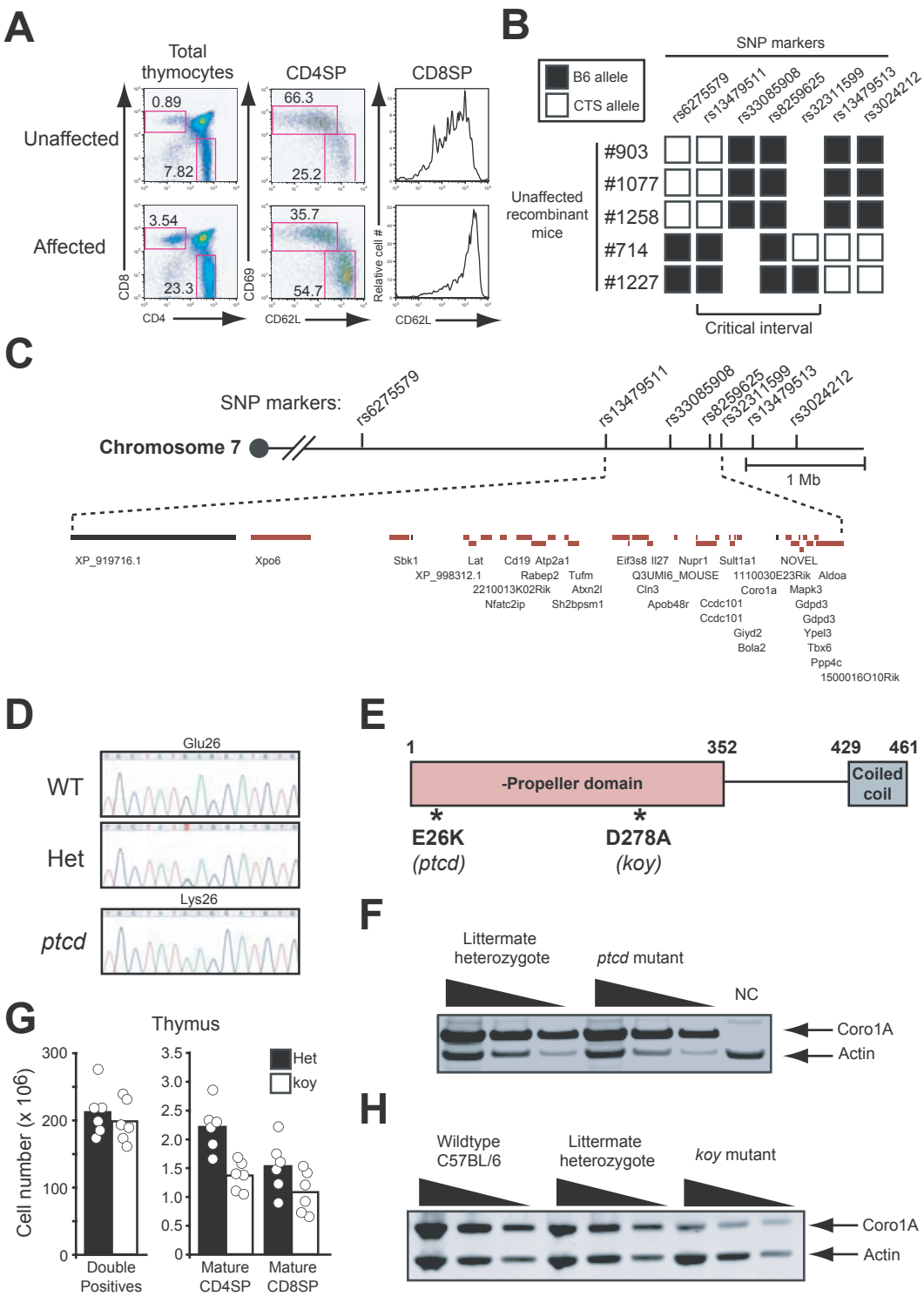
A
Total thymocytes
CD4SP
CD8SP
Unaffected
Affected
0.89
7.82
66.3
25.2
3.54
23.3
35.7
54.7
CD8
CD4
CD69
CD62L
Relative cell #
CD62L
B
B6 allele
CTS allele
SNP markers
rs6275579
rs13479511
rs33085908
rs8259625
rs32311599
rs13479513
rs3024212
#903
#1077
#1258
#714
#1227
Unaffected recombinant mice
Critical interval
C
SNP markers:
Chromosome 7
1 Mb
XP_919716.1
Xpo6
Sbk1
XP_998312.1
2210013K02Rik
Nfatc2ip
Lat
Cd19
Atp2a1
Rabep2
Tufm
Atxn2l
Sh2bpsm1
Eif3s8
Il27
Nupr1
Q3UMI6_MOUSE
Cln3
Apob48r
Sult1a1
1110030E23Rik
Coro1a
Ccdc101
Ccdc101
Giyd2
Bola2
NOVEL
Aldoa
Mapk3
Gdpd3
Gdpd3
Ypel3
Tbx6
Ppp4c
1500016O10Rik
D
Glu26
WT
Het
Lys26
ptcd
E
1
352
429
461
-Propeller domain
Coiled coil
E26K
(ptcd)
D278A
(koy)
F
Littermate heterozygote
ptcd mutant
NC
Coro1A
Actin
G
Thymus
Het
koy
Cell number (x 10^6)
300
200
100
0
3.5
3.0
2.5
2.0
1.5
1.0
0.5
0
Double Positives
Mature CD4SP
Mature CD8SP
H
Wildtype C57BL/6
Littermate heterozygote
koy mutant
Coro1A
Actin

Figure 2

Figure 3. E26K mutation alters Coro1A cellular distribution and causes irregularly shaped protrusions and reduced calcium flux. (A and B) Apoptosis assessment by **(A)** loss of mitochondrial membrane potential or **(B)** annexin-V staining of indicated cell types from wildtype, knockout and *ptcd* mutant mice following 4h incubation on ice (black) or at 37˚C (white). Pooled from three independent experiments. **(C)** Flow cytometric analysis of phalloidin binding in indicated cell types from wildtype, knockout and *ptcd* mice. Representative of at least three experiments. **(D)** Measurement of intracellular Ca^{2+} in the indicated cells from wildtype, knockout and *ptcd* mice; prebound antibodies to CD3 or CD3+CD4 were crosslinked by addition of streptavidin at the time indicated. Representative of three experiments. **(E to G)** T cells migrating on ICAM-coated coverslips in 1 ug/mL CCL21. Cells were stained for F-actin and (E) Coro1A or (F) Arp2/3 subunit p34. (G) Stills from brightfield time-lapse microscopy. White bar is 5 microns. Time in min and sec. Representative of three experiments. **(H)** Co-sedimentation assay of indicated purified Coronins and F-actin. S, supernatent. P, pellet. **(I)** Lysates from 293FT cells expressing indicated constructs were immunoprecipitated with anti-p34 and blotted with indicated antibodies. **(J)** Pulldown assay of indicated purified Coronins and blotting for the His-tagged Coronin or for p34. **(K)** Arp2/3-induced actin polymerization assay with indicated concentrations of purified Coronins. WT, wildtype coronin. E26K, mutant coronin. **(L)** T cells from *ptcd/+* and *ptcd/-* stained as in (E).

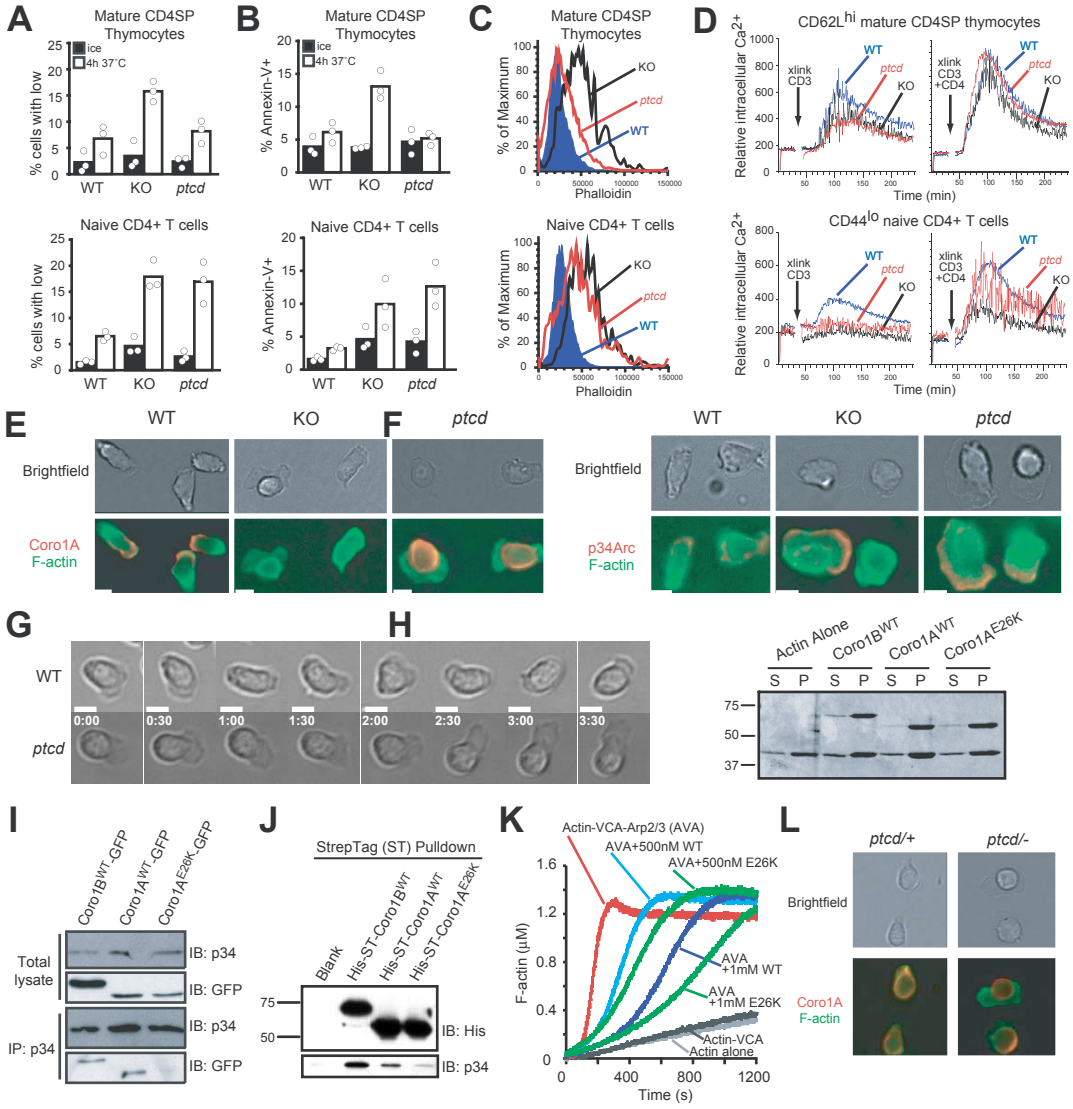
A
Mature CD4SP Thymocytes
ice
4h 37˚C
% cells with low
WT
KO
ptcd
Naive CD4+ T cells
B
Mature CD4SP Thymocytes
% Annexin-V+
Naive CD4+ T cells
C
Mature CD4SP Thymocytes
% of Maximum
KO
ptcd
WT
Phalloidin
Naive CD4+ T cells
D
CD62L^hi mature CD4SP thymocytes
Relative intracellular Ca2+
xlink CD3
xlink CD3 +CD4
Time (min)
CD44^lo naive CD4+ T cells
E
WT
KO
F
ptcd
Brightfield
Coro1A
F-actin
p34Arc
G
H
Actin Alone
Coro1B^WT
Coro1A^WT
Coro1A^E26K
S
P
75
50
37
I
Coro1B^WT-GFP
Coro1A^WT-GFP
Coro1A^E26K-GFP
Total lysate
IB: p34
IB: GFP
IP: p34
J
StrepTag (ST) Pulldown
Blank
His-ST-Coro1B^WT
His-ST-Coro1A^WT
His-ST-Coro1A^E26K
IB: His
K
Actin-VCA-Arp2/3 (AVA)
AVA+500nM WT
AVA+500nM E26K
AVA +1mM WT
AVA +1mM E26K
Actin-VCA
Actin alone
F-actin (μM)
Time (s)
L
ptcd/+
ptcd/-

Figure 3

Figure 4. Coronin-1A is mutated in a T-B+NK+ SCID patient. (A) Family pedigree and dideoxy sequence tracings from patient and family members, with red arrow indicating c.248delCT in patient that is heterozygous in father and leads to a premature truncation after 10 missense codons. **(B)** Western blot analysis for Coro1A and actin from EBV-transformed B cell lines derived from indicated subjects. Representative of three experiments. **(C)** Affymetrix SNP6.0 genechip analysis on buccal swap DNA from patient and mother.

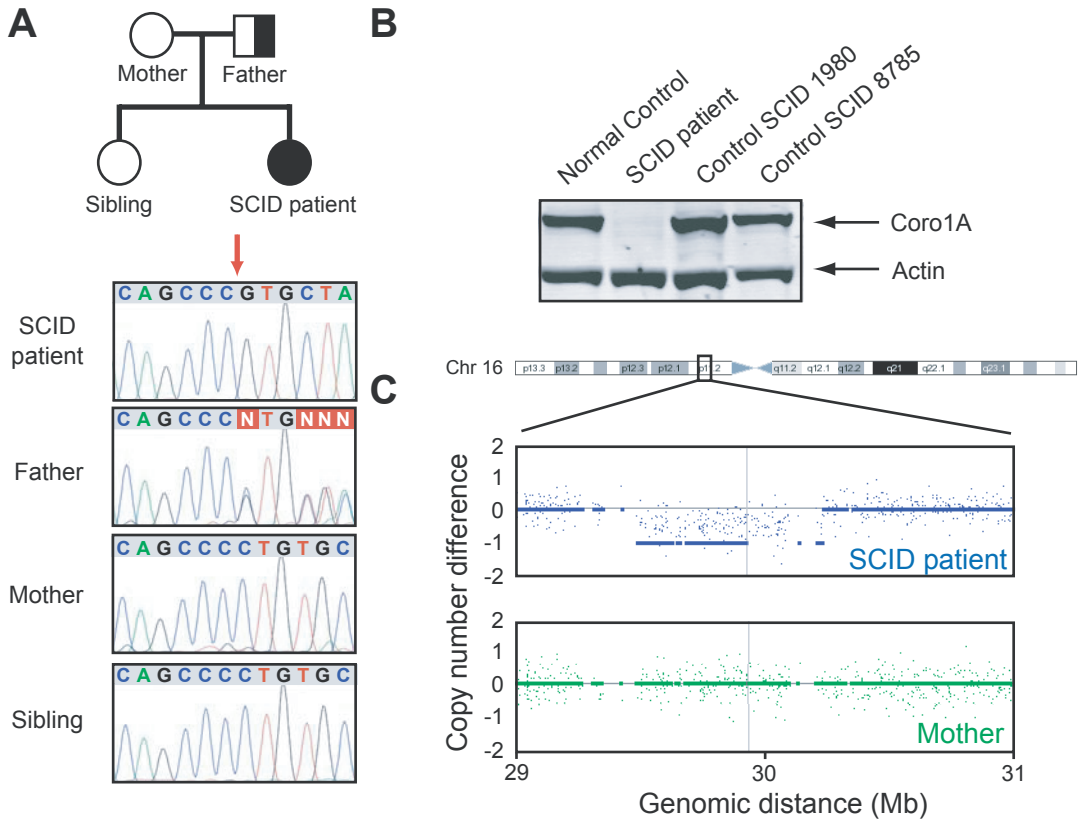
A
Mother
Father
Sibling
SCID patient
SCID patient
Father
Mother
Sibling
B
Normal Control
SCID patient
Control SCID 1980
Control SCID 8785
Coro1A
Actin
C
Chr 16
Copy number difference
SCID patient
Mother
Genomic distance (Mb)

Figure 4

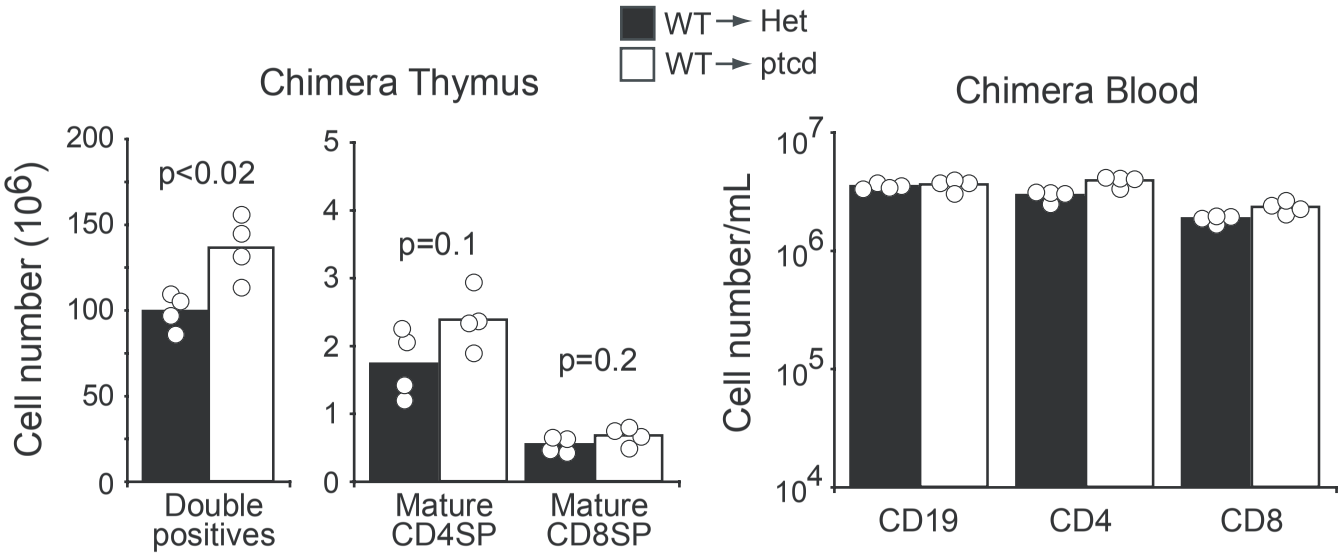

Figure S1. Lack of mature thymocyte accumulation and peripheral lymphopenia in reciprocal bone marrow chimeras. Thymocyte and blood lymphocyte subsets from ptcd (white) or control (black) mice reconstituted with wildtype bone marrow. Columns represent means and circles represent individual mice.

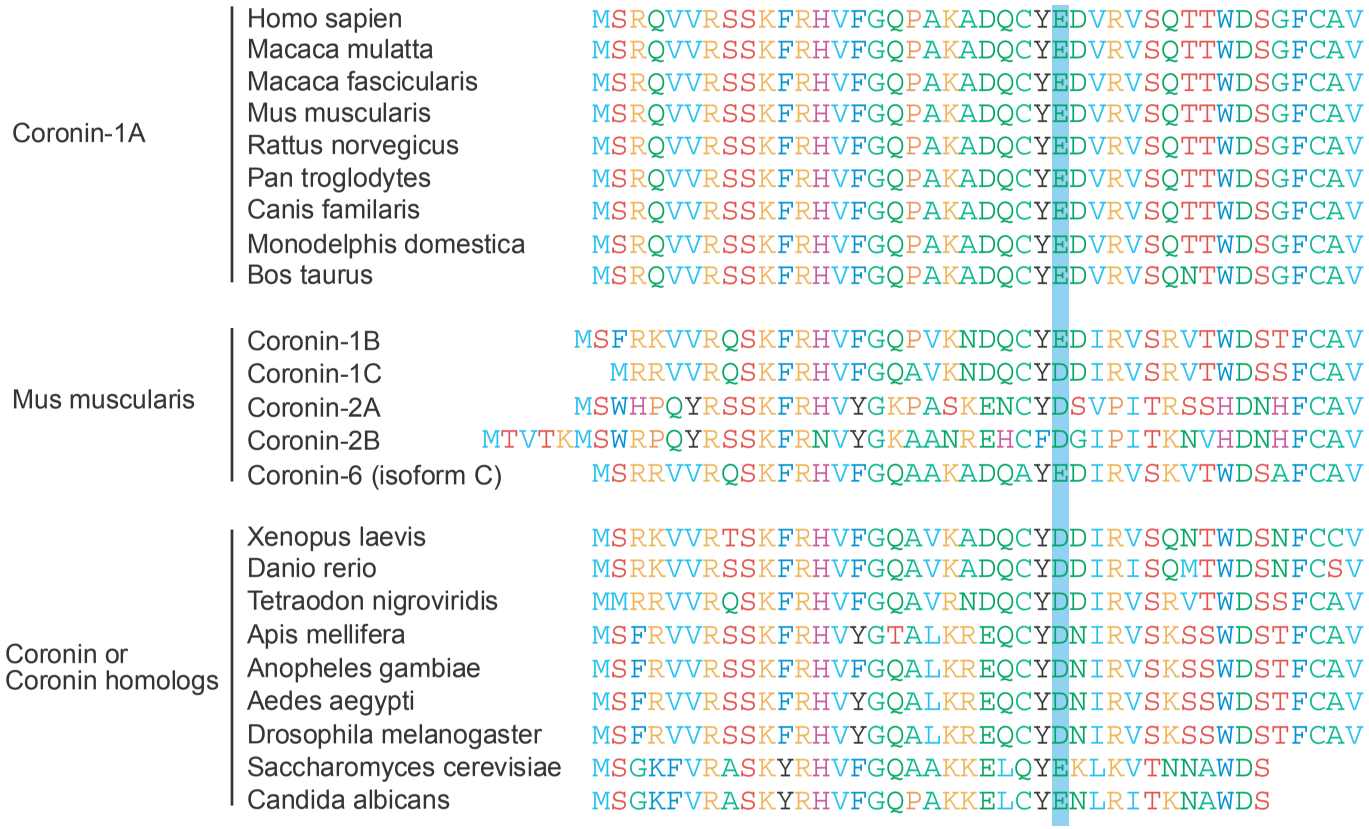

Figure S2. Conservation of glumatic acid at residue 26 in Coro1A and charge conservation across orthologs. Adapted from Polyphen and supplemented with additional sequences annotated in NCBI.

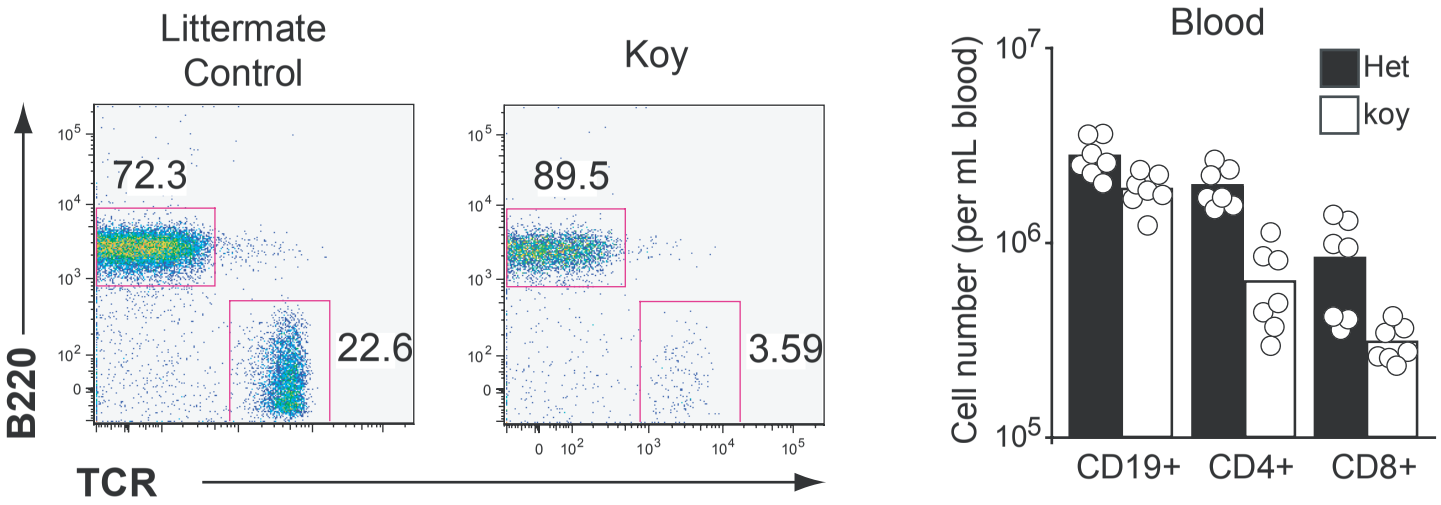

Figure S3. ENU-mutant Koyaanisquatsi (koy) identified as T-lymphopenic. (left) Flow cytometric analysis from peripheral blood of koy and littermate control mice demonstrated deficiency of TCR≤+ T lymphocytes. (right) Lymphocytes subsets in peripheral blood of koy (white) and control (black) mice. Columns represent means and circles represent individual mice.

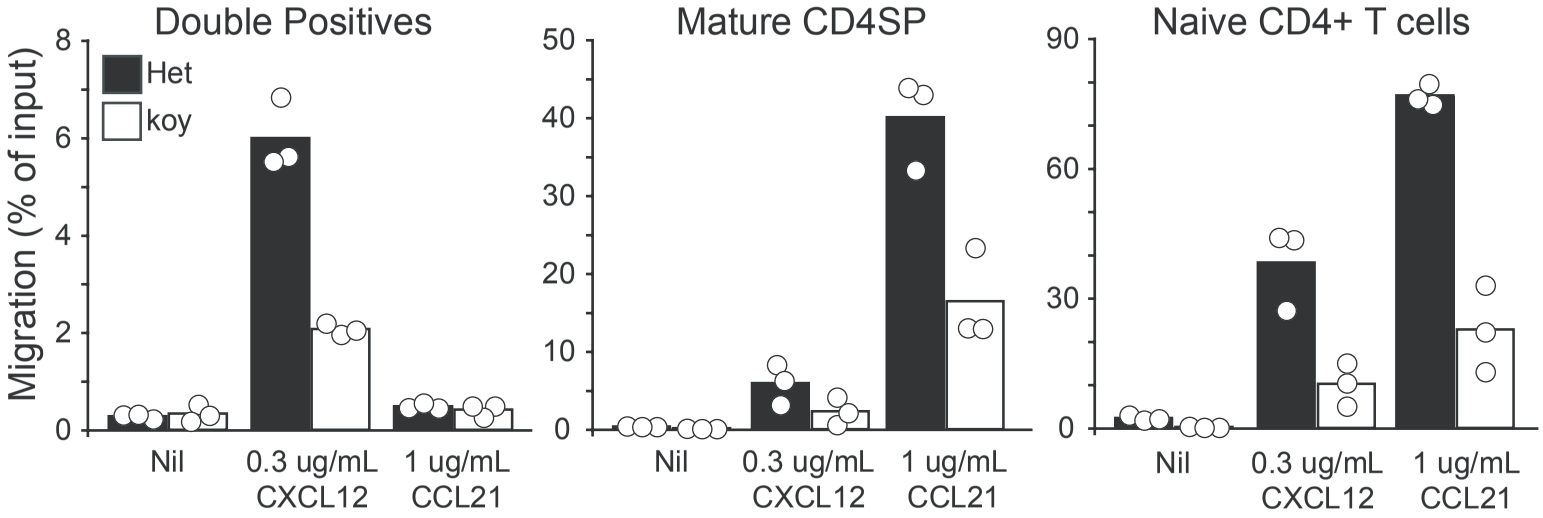

Figure S4. Migration defects in Koyaanisquatsi (koy) thymocytes and T cells. Transwell migration of koy (white) or control (black) DP thymocytes, mature CD4SP thymocytes or splenic naÔve CD4+T cell to indicated chemokines are shown as percentage of input that migrated. Columns represent means and circles represent individual mice pooled from three experiments.

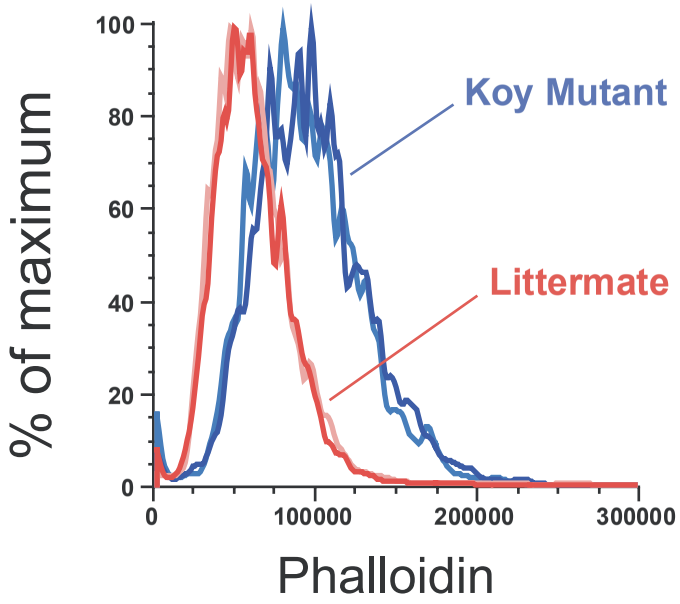

Figure S5. Elevated phalloidin staining in Koyaanisquatsi (koy) T cells. Flow cytometric analysis of phalloidin staining in mature CD4SP thymocytes from koy (blue lines) and control mice (red lines). Each line represents an individual mouse (two of each genotype). Representative of at least three independent experiments.

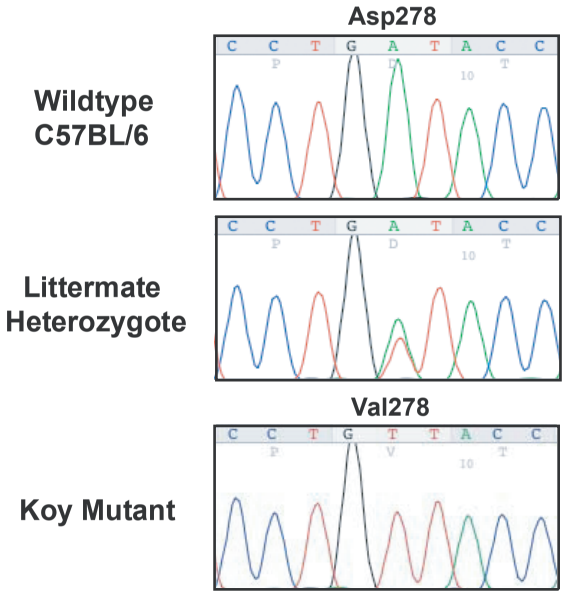

Figure S6. Point mutation in Coronin-1A in Koyaanisquatsi (koy) mice. Dideoxy sequence tracings from genomic tail DNA of koy and control mice for Coro1A demonstrating D278V point mutation.

Supplementary Movie S1. Comparison of two-photon time-lapse microscopy of control (left) or *ptcd* (right) cells labeled in red and wildtype GFP cells in green migrating in the T zone of an explanted lymph node. Yellow tracks generated to aid visualization of representative wildtype GFP cells and white tracks of control (left) or *ptcd* (right) cells.

Supplementary Movie S2. Brightfield time-lapse microscopy of widltype lymph node cells on ICAM-coated coverslips in 1 ug/mL CCL21, followed by fluorescent exposure to identify T cells (blue), B cells (red) and dead cells (pink). Tracks generated to aid visualization of migrating T cells. Movie is optimally viewed at full-screen.

Supplementary Movie S3. Brightfield time-lapse microscopy of mutant *ptcd* lymph node cells as described in Movie 2.

Supplementary Movie S4. Comparison of brightfield time-lapse microscopy of wildtype and mutant *ptcd* T cells cropped from Movies 2 and 3.

Supplementary Movie S5. Brightfield time-lapse microscopy of Coro1A-/- lymph node cells as described in Movie 2.

Primer Name	Sequence	Sequencing	Genomic qPCR
hCoro1A-R1	CAGCCTCTCCTTCCCTCTAAC		intron 1-2
hCoro1A-F2	CACGCCAGGCTCTGTTG	Exon 2	intron 1-2
hCoro1A-R2	CGGGTTGTTCTTCTCTTGTTC	Exon 2	intron 2-3
hCoro1A-F3	CCTAAGGGCAGAGACAGACTG	Exons 3-6	intron 2-3
hCoro1A-R3	CACGCCTGGGTAAACTGA	Exons 3-6	intron 6-7
hCoro1A-F4	ACCAAGACTGGAGGTTTCGTC	Exons 7-11	intron 6-7
hCoro1A-R4	CTGGGAATGGGAGGTGAGT	Exons 7-11	exon 11
hCoro1A-F5	GACAGGCTGGAGGAGACAG		exon 11
hGAPDH-F	GTTCCAATATGATTCCACCC		exon 4
hGAPDH-R	GAAGATGGTGATGGGATTTC		exon 4
hCoro7-F	AGAGTTCTTCCAGGATGACG		exon 25
hCoro7-R	AGGCTGAGAAGCCAGGG		exon 25
hEdg1-F	AGCGGAGACTCTGCTGG		exon 2
hEdg1-R	CTGGGGGTGGGAGGAAT		exon 2

Table S1. Primers used for quantitative PCR and sequencing of human genomic DNA.

CHAPTER 4

Conclusions and Discussion

CD69 & $S1P_1$

Our work demonstrates that CD69 inhibits sphingosine-1-phosphate receptor 1 ($S1P_1$) to rapidly block lymphocyte egress following activation by type I interferons (IFNα/β).

While CD69 inhibition of $S1P_1$ can account for much of the lymphocyte intrinsic mechanism of lymph node shutdown, additional extrinsic mechanisms may affect the $S1P_1$ egress pathway. A recent study has demonstrated that a balance between $S1P_1$ egress and chemokine retention signals dictate the rate of lymphocyte egress[1]. A possible additional mechanism for lymph node shutdown could be retention through increased chemokine expression. Indeed, changes in lymph node homeostatic chemokine levels have been observed following viral immune responses[2]. However, these are decreases occurring over many days and rely on CD4+ T cell production of IFNγ. In a separate study on the retention of CD8+ T cells in responding lymph nodes, dendritic cells were shown to attract the CD8+ T cells through chemokine production[3]. It remains to be seen whether chemokine availability can modulate during lymph node shutdown.

An increase in tissue S1P could also block lymphocyte egress by disrupting the S1P gradient. Augmentation of S1P levels could occur through either increased S1P production or decreased breakdown of S1P. Changes in S1P levels have been reported in peripheral tissues days following acute inflammatory conditions[4]. Future studies should determine whether S1P levels acutely change within lymphoid organs during lymph node

shutdown. Finally, there are likely additional extrinsic mechanisms contributing to lymph node shutdown that do not affect lymphocyte $S1P_1$, such as potential constraints by the lymphatic endothelium on lymphocyte exit sites.

Further studies should also determine the role of CD69 in regulating migration and egress following activation by antigen receptors. Real-time imaging of lymph nodes with two-photon microscopy has described three distinct phases of T cell migratory behaviors with antigen-presenting cells[5]. During the first phase (~8 h), T cells searching for cognate antigen rapidly migrate and form short-lived contacts with dendritic cells (DCs). In phase 2 (8 -24 h), T cells migrate more slowly and form prolonged contacts with DCs. This change in behavior by T cells between the first two phases occurs through a T cell intrinsic mechanism[6]. Interestingly, CD69 upregulation occurs during phase 2[5]. In phase 3 (after 24 h), T cells reduce their length of contact with DCs, gradually downmodulate CD69, and begin to proliferate. A separate group has also observed a similar reduction in migration by T cells when presented tolerance-inducing levels of antigen[7].

Based on this priming model, CD69 dependent as well as independent mechanisms could contribute to migratory behaviors as well as lymph node retention. During phase 1, CD69 may provide the early stop signal for progression into phase 2. Whether or not CD69 contributes to other T cell migratory behaviors during phase 2 remains to be tested. On the other hand, a strong TCR signal may serve as a sufficient

retention mechanism either through transcriptional downmodulation of $S1P_1$ or through integrin enforced synapse conjugates. Furthermore, changes in the chemokine receptors or local chemokine milieu may contribute to retention.

Recent work describes asymmetric cell division occurring at the initial stage of T cell proliferation[8]. The proximal daughter cell, defined by having greater synaptic receptors, displays more CD69 and is thought to have an effector fate. The distal daughter cell has less CD69 and is thought to have a memory fate. It is unclear whether or not this partition in CD69 plays a functional role in the differences between the two daughter cells. Alternatively, $S1P_1$ could also asymmetrically partition and CD69 may simply reflect that difference. Of note, CD69 surface expression remained high on memory follicular helper T cells retained in lymphoid organs[9].

Aside from lymphocyte egress, CD69 may also be regulating other $S1P_1$ functions. In marginal zone (MZ) B cells, $S1P_1$ is required for localization to the splenic MZ[10]. Recent work using an *in vivo* labeling technique has demonstrated that MZ B cells are constantly shuttling between the MZ and follicle, and that a balance between CXCR5 and $S1P_1$/$S1P_3$ signaling mediates this shuttling[11]. Upon stimulation with TLR4 agonist LPS, MZ B cells will rapidly downmodulate $S1P_1$ transcripts and localize to the follicle[10]. While poly(I:C) treatment also induces MZ B cell migration into the follicle, MZ B cells do not downmodulate $S1P_1$ transcript but do upregulate CD69[12]. This suggests that MZ B cells also transiently induce CD69 as a mechanism to regulate $S1P_1$ when activated

indirectly through IFNα/β. Further studies could confirm this notion by applying the *in vivo* MZ-labeling technique to mice genetically deficient of CD69.

In addition to regulating lymphocyte positioning, CD69 may have additional contributions through its interaction with other S1P receptors. Many cell types express CD69 including NK cells and platelets. $S1P_5$ regulates NK cell trafficking and CD69 may play a role in regulating its function. Platelets can release S1P and also become activated by it[13]. The receptor that mediates S1P actiation on platelets is unclear. Studies using human platelets have also demonstrated that CD69 crosslinking with mAb can lead to activation[14]. Thus, CD69 could play a role in S1P receptor regulation in other hematopoetic cell types.

Beyond inhibiting $S1P_1$ function, CD69 may also be utilizing its unique association with $S1P_1$ for G^i-dependent signaling. An immunoprecipitation of CD69 from activated T cell showed that it associated a molecule that could be labeled by pertussis toxin[15]. Furthermore, degranulation in mast cell lines using CD69 mAb crosslinking can be inhibited by pertussis toxin[16]. Calcium signaling in effector T cells has been rescued by CD69 mAb crosslinking, and this effect is pertussis toxin sensitive[17]. These studies suggest that CD69 mediate effects through coupling with G_i. Since CD69 lacks a signaling motif in its cytoplasmic tail, it may be coupling to G_i through $S1P_1$.

Understanding a potential CD69-$S1P_1$ signaling complex requires better characterization of their interaction. The RAMP family is another example of single-transmembrane receptors associating with and modulating GPCRs[18]. Studies have dissected the contribution of different RAMP domains and revealed additional RAMP functions in internalization and recycling[19]. It will be important to determine which domains of CD69 are involved in interaction with $S1P_1$. A transgenic mouse expressing CD69 with a cytoplasmic trunction was still capable of inhibiting thymic egress[20]. Furthermore, our data shows that $S1P_1$ could still associate with a CD69 chimera in which the cytoplasmic domain is replaced by CD3ζ signaling motifs. Thus the cytoplasmic domain is not likely critical for the CD69-$S1P_1$ association. RAMP family members also modulate the ability of GPCRs to associate with their ligand, and it will be interesting to study the effects of CD69 on S1P binding. Future studies should also explore whether a direct interaction exists and how $S1P_1$ functional inhibition occurs.

Since its discovery two decades ago, CD69 has served as a useful marker for cell activation but its function remained elusive. Now, with an established role in lymphocyte migration and its association with a G-protein coupled receptor, CD69 may further reveal additional functions while serving as a model for studying related C-type lectins.

Coronin-1A in T cell and actin biology

We have identified Coronin-1A mutations in a spontaneous thymic egress mutant mouse and in an atypical patient with T-B+NK+ SCID. Our work extends the role of actin regulation by Coronin-1A to thymic and lymph node egress by T cells, and links Coro1A to a human immunological disease.

Coronin was first described in the slime mold Dictyostelium as an actin-associated protein that formed a "crown-like" structure on electron microscopy[21]. Deletion of coronin in Dictyostelium causes defects in multiple actin-associated processes including phagocytosis, cytokinesis and migration[22, 23]. In yeast, the coronin homolog Crn1 was shown to interact with and inhibit Arp2/3[24]. Electron microscopic analysis of purified proteins showed direct interaction of Crn1 with an inactive form of Arp2/3[25]. Thus, a model emerged from these studies in which coronin could inhibit Arp2/3 activity through their direct interaction.

In mammals, there are multiple coronin isoforms including Coro1A, which has a hematopoeitic-restricted expression pattern. From macrophage and neutrophils, Coro1A was initially extracted, respectively, from phagosomes and NADPH-oxidase complexes[26, 27]. In the human Jurkat T cell line, Coro1A can be detected near the leading edge during migration as well as at the immune synapse[28]. The localization of Coro1A to this structure suggests its role in formation of the immune synapse.

Surprisingly, the first Coro1A-/- study from Foger et al. reported a normal formation of the T cell immunological synapse as well as normal responses to antigen-induced TCR stimuli[29]. The authors did find both migration and survival defects in Coro1A-/- naïve T cells and attributed these defects to an over-accumulation of F-actin from unchecked Arp2/3 activity[29]. However, two papers also reporting mice with Coro1A deficiency followed with conflicting conclusions[30, 31].

In an effort to identify lupus susceptibility genes in mice, Haraldsson et al. conversely identified a "lupus suppressing" Lmb3 locus containing a spontaneous null allele of Coro1A[30]. With their Lmb3 mutant mouse, which differs in strain background from mice studied by Foger et al., Haraldsson et al. also reported naïve T cell survival and migration defects with elevated F-actin. However, Lmb3 mice had defects in calcium signaling and cell proliferation following TCR-crosslinking[30]. These results conflict with normal TCR signaling results in the Foger et al. study.

In Mueller et al, the authors also generated a gene targeted Coro1A-/- mouse and reported T cell survival defects. Interestingly, these authors insist that F-actin levels are not altered and argue that Coro1A-/- T cells do not have a migration defect. In agreement with the Lmb3 findings, Mueller et al. also found a naïve T cell proliferation and calcium signaling defects following TCR-crosslinking. They attributed these defects to a requirement for Coro1A to interact with phospholipase-C gamma (PLCγ) following TCR

stimulation. They further conclude that defective TCR signaling, rather than F-actin accumulation, renders naïve T cells susceptible to death.

These three studies, with partially conflicting conclusions, pose several questions. Why did the Foger et al. study not detect any TCR signaling defect? How does Coro1A function in TCR signaling? Is F-actin affected in Coro1A mutants? How does the lack of Coro1A lead to these multiple defects?

A key difference in the TCR signaling studies by Foger et al. is the use of the DO11.10 TCR transgene to stimulate T cells with APCs pulsed with OVA peptide. In the other two studies, T cells were stimulated with mAb that crosslinked the TCR. The authors from both of these studies suggested that the fixed TCR alters the naïve T cell, causing the transgenic T cells to behave more effector-like. An alternative possibility is that the peptide stimulation, with the MHC contextually presented by the APC, signals the TCR in a Coro1A-independent manner. Consistent with this latter hypothesis, our calcium signaling experiments using both Coro1A-/- and Coro1A^{E26K} T cells demonstrate a qualitative recovery when TCR-crosslinking is coupled with CD4-crosslinking to mimic MHC engagement.

The role of Coro1A in TCR signaling remains unclear, but can be represented by two models: direct and indirect. The direct model, supported by Mueller et al, argues that Coro1A acts directly in the TCR signaling pathway, perhaps at the proximal level of IP3

production by PLCγ1. This direct model is an attempt to explain an actin-independent mechanism for Coro1A. However, the direct model can also involve an actin-regulatory function of Coro1A. The localization of Coro1A to the immune synapse, as well as the requirement for other actin-associated molecules in TCR signaling, support this notion.

In the indirect model, suggested by Haraldsson et al, Coro1A deficiency disrupts the naïve T cell's actin turnover and this cytoskeletal disruption impairs calcium mobilization downstream of TCR signaling. One possible calcium mobilization step that Coro1A deficiency may disrupt is the link between the Stim calcium sensing proteins and the Orai calcium channels. Imaging studies have shown that Stim1 in the ER membrane dynamically moves on microtubules[32, 33] and a malformation in the actin cytoskeleton could possibly impair proper microtubule assembly or hinder Stim1 motility. An important approach for future studies is to examine non-TCR calcium signaling in Coro1A deficient T cells.

The model proposed by Mueller et al. is formed by two conclusions – Coro1A is required for IP3 production by PLCγ1 and Coro1A deficiency does not alter F-actin turnover. However, the subtle decrease in IP3 production that the authors observed in Coro1A-/- T cells may have been confounded by the survival defect. Isolated T cells not only spent time undergoing purification from bulk spleen preparations, but were also serum starved for hours in vitro prior to the IP3 assay. A difference in IP3 production could simply reflect the cell death that occurred. We have observed that both Coro1A-

deficient and Coro1A^{E26K} naive T cells undergo apoptosis within hours. The intriguing co-immunoprecipitation of Coro1A with PLCγ1 may reflect a novel interaction but PLCγ1 was pulled down in the absence of TCR-stimulation. Future studies should confirm that PLCγ1 can indeed interact with Coro1A in the context of TCR signaling.

The argument by Mueller et al. regarding normal F-actin content in Coro1A-/- T cells draws from various observations, each with its own caveats. First, they observe protrusions of plate bound T cells responding to TCR stimuli and observe no difference between wildtype and Coro1-/-. They further refer to normal migration and phagocytosis in Coro1A-/- macrophages[34]. Together, they conclude that Coro1A deficiency has not affect F-actin processes, but fail to consider that actin dynamics in migration differs from TCR-induced actin dynamics and that macrophages express additional coronin molecules such as Coro1B. Next, their conclusions on the lack of F-actin accumulation in Coro1A-/- T cells is based on biochemical data with questionable sensitivity compared to flow cytometric phalloidin staining. Furthermore, they note that other lymphocyte subsets exhibit elevated phalloidin staining but lack a survival defect, and conclude that the phalloidin staining fails to reflect an actual increase in F-actin. However, a possible explanation is that the elevated F-actin promotes apoptosis differentially in lymphocyte subsets. B and T cells, as well as their immature progenitors, indeed express different apoptotic genes and exhibit different propensities for cell death.

Finally, our assessment of *ptcd* T cells is not consistent with the model proposed by Mueller et al. T cells from *ptcd* mice have migration and trafficking defects, along with abnormal actin protrusions when stimulated to migrate *in vitro*. Furthermore, the phalloidin staining of *ptcd* T cells revealed an intermediate but still elevated F-actin level, and provided an allelic difference for comparison of calcium signaling and survival. While calcium signaling is still impaired in *ptcd* T cells, cell survival is notably attenuated and correlates with the partial phalloidin staining. Thus, our data fails to support the direct model by Mueller et al. and is consistent with the model proposed by Foger et al.

Further clarity on the role of Coro1A in T cell biology may come from understanding its mechanisms for actin regulation. Much of the biochemical insight on mammalian coronin function has been based on studies with Coro1B, an isoform that is ubiquitously expressed and is closely related to Coro1A. Coro1B association with Arp2/3 depends on its C-terminal coiled-coiled domain as well as its phosphorylation state at residue Ser2[35], and these interaction properties are conserved with Coro1A[29]. In addition, Arg30 is required for Coro1B binding to F-actin[36]. While the E26K mutation found in *ptcd* mice is located proximal to this Arg residue (at position 29 in Coro1A), the F-actin binding of Coro1A^{E26K} is surprisingly not impaired. However, purified Coro1A^{E26K} fails to efficiently associate with Arp2/3. The Glu26 may share a common domain or surface with the Ser2 containing N-terminus. Unfortunately, the first seven residues of the Coro1A crystal structure were unresolvable[37]. Future studies should

explore the role of Glu26 in the Ser2 phosphorylation dependent association between Coro1A and Arp2/3.

The model based on yeast Crn1 explains coronin inhibition of Arp2/3 by direct contact and would predict the E26K mutation to attenuate Coro1A inhibition of Arp2/3. Surprisingly, Coro1A^{E26K} is more potent at inhibiting Arp2/3 branching activity in an *in vitro* pyrene assay. This result indicates that Coro1A can inhibit Arp2/3 activity through an indirect mechanism likely involving F-actin binding. This new model is further supported by evidence that the F-actin binding mutant Coro1B^{R30D} can normally associate with Arp2/3 but fails to inhibit Arp2/3 activity (personal communication Cai and Bear). Together, these results suggest that mammalian coronin inhibits Arp2/3 through an indirect mechanism that relies on F-actin association.

In addition to Arp2/3 and F-actin, Coro1A is likely forming complex interactions *in vivo* with other actin-associated molecules in T cells. Coro1B associates with Slingshot[38], a phosphatase that actives the actin-severing protein cofilin[39]. Slingshot can also dephosphorylation Coro1B and its subcellular localization depends on Coro1B[38]. Coro1A molecules that associate with F-actin may also share binding regions with cortactins or formins. These families of actin-associated molecules have homologs (HS1 and mDia1) critical for T cell actin biology[40, 41]. It is possible that Coro1A may associate in different actin regulatory modules that contribute to the various T cell processes of migration, signaling and survival.

It remains unclear why Coro1A^{E26K} is aberrantly mislocalized in migrating T cells. While its *in vitro* sedimentation with F-actin is not altered, the *in vivo* association of Coro1A^{E26K} with F-actin may be different. Unlike *in vitro* F-actin, the F-actin *in vivo* could be differentially coupled to GTP and GDP, form diverse bundles or be decorated by different actin-associated molecules. These differences could possibly alter F-actin conformation and affect Coro1A association. Another possibility is that Coro1A^{E26K} fails to interact with an unknown protein, leading to sequestration away from or failure to access the leading edge.

Better understanding of the molecular roles of Coro1A and other actin regulatory components during dynamic T cell migration may provide further clarity on the *ptcd* T cell trafficking phenotype. While *ptcd* T cells have a marked thymic accumulation, trafficking through lymph nodes is not as dramatically affected. Both entry into and exit from lymph nodes were only reduced two-fold. Also, the velocity of ptcd T cells within the lymph node was only partially reduced. In vitro assays have not been fully informative in understanding this discrepancy. While transwell migration assays show a marked reduction towards chemokines and S1P, real-time imaging on two-dimensional ICAM surfaces has revealed that *ptcd* T cells have aberrant protrusions but still displace.

One possible explanation would speculate that the thymic exit structure places greater demand on Coro1A-dependent F-actin regulation. Thymic egress is thought to occur through corticomedullary vessels where reverse transmigration could take place

from the thymic tissue into a higher-pressure blood vessel. A tight blood-thymus barrier exists and may function to prevent circulating antigens from entering the thymus. In contrast, the lymph node does not need such a tight barrier against circulating fluids because it function to filter antigens from fluids. Thus, the high-endothelial venules (HEVs) would not necessarily need to form a tight barrier. Furthermore, the LYVE1+ lymphatic endothelial exit structures in the lymph node also differ in that the lymph fluid has lower pressure than blood. Thus, it is possible that mature T cells exiting the thymus must navigate a tighter and less forgiving endothelial barrier than either HEVs or LYVE1+ lymphatic exit sites. This would also be consistent with *ptcd* T cells failing to migrate across transwells with five-micron diameter pores that may require the cell to actively protrude.

While our study contributes to our growing understanding of Coro1A, there are still many questions to answer regarding its role in T cell and actin biology. Future approaches may reveal further insights to actin biology through studies on novel thymic egress mutants. And likewise, our understanding of T cell egress will grow as molecular mechanisms for coronin and actin cytoskeleton regulation are further uncovered.

Coronin-1A and human SCID

Severe combined immunodeficiency (SCID) describes a group of genetic disorders impairing both humoral and cell-mediated adaptive immunity[42]. The incidence of SCID, likely under diagnosed, varies worldwide from 1 in 50,000 to 1 in 1,000,000[43]. The most common form is X-linked SCID, caused by mutations in cytokine receptor common gamma chain[44]. With a halt on gene therapy trials[45], the only treatment currently available to SCID patients is bone marrow transplantation.

SCID can be caused by mutations that impair both T and B lymphocytes, but T-B+ NK+ SCID classifies a subset of patients with T cell deficiency but relatively normal B and NK cell numbers. To date, genetic causes of T-B+NK+ SCID have been defects in two major pathways: TCR or interluekin(IL) -7 cytokine signaling pathways. Defects can start upstream of the TCR with mutations affecting MHC molecules, as in bare lymphocyte syndromes[46]. Various genetic defects within the TCR complex have been described including CD3ε, CD3δ, CD3γ[47]. Finally, defects in genes that affect proximal signals downstream of the TCR complex have been reported as well, including Zap70[48, 49], Lck[50, 51], and CD45[52, 53]. With IL-7 cytokine signaling, mutations in Jak3, a kinase downstream of IL-7 receptor (IL-7R), were find in autosomal recessive forms of T-B+NK+SCID[54, 55]. Later, mutations abrogating IL-7R expression were also discovered[56]. To date, these two signaling pathways (TCR and IL-7R) have accounted for all known cases of T-B+NK+ SCID.

Our study reports a Coro1A deficiency associated with T-B+NK+ SCID. While the precise role of Coro1A remains untested in human T cells, the data from mouse studies does not indicate that Coro1A primarily functions downstream of TCR or cytokine signaling pathways. However, the effects of Coro1A on the actin cytoskeleton may have indirect effects on TCR and cytokine-dependent survival signals. Future studies on T cells from other T-B+NK+ SCID patients with Coro1A deficiency will likely provide important insights towards understanding the function of coronin in humans.

Unlike most cases of T-B+NK+ SCID, the patient we've described had an atypical presentation. While most SCID patients present between 6 mo and 1 yr of life, our patient did not have any severe infections in the first year of life. She developed a severe varicella infection involving skin and mucous membranes only after receiving a varicella vaccination. This vaccine is composed of the live attenuated Oka strain [57] and is contraindicated against immunocompromised patients. Incidents of post-vaccination disseminated varicella have been reported in both primary and acquired immunodeficient children[58, 59]. In one example, a child with adenosine deaminase deficiency had previously presented in the first year of life with chronic diarrhea, chronic thrush, and multiple episodes of bronchiolitis[58].

The genetic defect underlying the Coro1A deficiency is also unique. While one allele with the 2bp coding deletion was inherited from the father, the other allele carries a

microdeletion in 16p11.2 that encompasses Coro1A. The mother lacks this microdeletion, suggesting that it occurred de novo. Interestingly, multiple groups have reported this exact microdeletion in association with autism[60-62]. Additional copy number variations have also been reported in this region of chromosome 16[63-65]. Based on a population analysis in Iceland, the incidence of this microdeletion has been reported as 1% in autism, 0.1% in patients with psychiatric disorders, and 0.01% in the general population[61]. Therefore, we predict that additional cases of Coro1A-deficiency may involve this 16p11.2 microdeletion.

Unknown causes for SCID account for roughly 15% of cases[42], with many involving de novo mutations or small family cohorts. Recently, population studies have yielded genetic linkages to many common polygenic disorders. However, these SNP-based approaches are not useful for SCID, which has a low frequency and is typically caused by single gene defects. Instead, forward genetics in mouse and copy-number variation analysis in humans can help identify unique genetic defects in rare diseases. Future studies of this type may yield additional genes involved in the Coro1A-dependent pathways for T cell survival or migration.

References:

1. Pham, T. H., Okada, T., Matloubian, M., Lo, C. G. & Cyster, J. G. S1P1 receptor signaling overrides retention mediated by G alpha i-coupled receptors to promote T cell egress. Immunity 28, 122-33 (2008).

2. Mueller, S. N. et al. Regulation of homeostatic chemokine expression and cell trafficking during immune responses. Science 317, 670-4 (2007).

3. Castellino, F. et al. Chemokines enhance immunity by guiding naive CD8+ T cells to sites of CD4+ T cell-dendritic cell interaction. Nature 440, 890-5 (2006).

4. Ledgerwood, L. G. et al. The sphingosine 1-phosphate receptor 1 causes tissue retention by inhibiting the entry of peripheral tissue T lymphocytes into afferent lymphatics. Nat Immunol 9, 42-53 (2008).

5. Mempel, T. R., Henrickson, S. E. & Von Andrian, U. H. T-cell priming by dendritic cells in lymph nodes occurs in three distinct phases. Nature 427, 154-9 (2004).

6. Henrickson, S. E. et al. T cell sensing of antigen dose governs interactive behavior with dendritic cells and sets a threshold for T cell activation. Nat Immunol 9, 282-91 (2008).

7. Shakhar, G. et al. Stable T cell-dendritic cell interactions precede the development of both tolerance and immunity in vivo. Nat Immunol 6, 707-14 (2005).

8. Chang, J. T. et al. Asymmetric T lymphocyte division in the initiation of adaptive immune responses. Science 315, 1687-91 (2007).

9. Fazilleau, N. et al. Lymphoid reservoirs of antigen-specific memory T helper cells. Nat Immunol 8, 753-61 (2007).

10. Cinamon, G. et al. Sphingosine 1-phosphate receptor 1 promotes B cell localization in the splenic marginal zone. Nat Immunol 5, 713-20 (2004).

11. Cinamon, G., Zachariah, M. A., Lam, O. M., Foss, F. W., Jr. & Cyster, J. G. Follicular shuttling of marginal zone B cells facilitates antigen transport. Nat Immunol 9, 54-62 (2008).

12. Rubtsov, A. V. et al. TLR agonists promote marginal zone B cell activation and facilitate T-dependent IgM responses. J Immunol 180, 3882-8 (2008).

13. Yatomi, Y., Ruan, F., Hakomori, S. & Igarashi, Y. Sphingosine-1-phosphate: a platelet-activating sphingolipid released from agonist-stimulated human platelets. Blood 86, 193-202 (1995).

14. Testi, R., Pulcinelli, F., Frati, L., Gazzaniga, P. P. & Santoni, A. CD69 is expressed on platelets and mediates platelet activation and aggregation. J Exp Med 172, 701-7 (1990).

15. Risso, A. et al. CD69 in resting and activated T lymphocytes. Its association with a GTP binding protein and biochemical requirements for its expression. J Immunol 146, 4105-14 (1991).

16. Sancho, D. et al. Functional analysis of ligand-binding and signal transduction domains of CD69 and CD23 C-type lectin leukocyte receptors. J Immunol 165, 3868-75 (2000).

17. Bikah, G., Pogue-Caley, R. R., McHeyzer-Williams, L. J. & McHeyzer-Williams, M. G. Regulating T helper cell immunity through antigen responsiveness and calcium entry. Nat Immunol 1, 402-12 (2000).

18. McLatchie, L. M. et al. RAMPs regulate the transport and ligand specificity of the calcitonin-receptor-like receptor. Nature 393, 333-9 (1998).

19. Parameswaran, N. & Spielman, W. S. RAMPs: The past, present and future. Trends Biochem Sci 31, 631-8 (2006).

20. Nakayama, T. et al. The generation of mature, single-positive thymocytes in vivo is dysregulated by CD69 blockade or overexpression. J Immunol 168, 87-94 (2002).

21. de Hostos, E. L., Bradtke, B., Lottspeich, F., Guggenheim, R. & Gerisch, G. Coronin, an actin binding protein of Dictyostelium discoideum localized to cell surface projections, has sequence similarities to G protein beta subunits. Embo J 10, 4097-104 (1991).

22. de Hostos, E. L. et al. Dictyostelium mutants lacking the cytoskeletal protein coronin are defective in cytokinesis and cell motility. J Cell Biol 120, 163-73 (1993).

23. Maniak, M., Rauchenberger, R., Albrecht, R., Murphy, J. & Gerisch, G. Coronin involved in phagocytosis: dynamics of particle-induced relocalization visualized by a green fluorescent protein Tag. Cell 83, 915-24 (1995).

24. Humphries, C. L. et al. Direct regulation of Arp2/3 complex activity and function by the actin binding protein coronin. J Cell Biol 159, 993-1004 (2002).

25. Rodal, A. A. et al. Conformational changes in the Arp2/3 complex leading to actin nucleation. Nat Struct Mol Biol 12, 26-31 (2005).

26. Ferrari, G., Langen, H., Naito, M. & Pieters, J. A coat protein on phagosomes involved in the intracellular survival of mycobacteria. Cell 97, 435-47 (1999).

27. Grogan, A. et al. Cytosolic phox proteins interact with and regulate the assembly of coronin in neutrophils. J Cell Sci 110 (Pt 24), 3071-81 (1997).

28. Nal, B. et al. Coronin-1 expression in T lymphocytes: insights into protein function during T cell development and activation. Int Immunol 16, 231-40 (2004).

29. Foger, N., Rangell, L., Danilenko, D. M. & Chan, A. C. Requirement for coronin 1 in T lymphocyte trafficking and cellular homeostasis. Science 313, 839-42 (2006).

30. Haraldsson, M. K. et al. The Lupus-Related Lmb3 Locus Contains a Disease-Suppressing Coronin-1A Gene Mutation. Immunity 28, 40-51 (2008).

31. Mueller, P. et al. Regulation of T cell survival through coronin-1-mediated generation of inositol-1,4,5-trisphosphate and calcium mobilization after T cell receptor triggering. Nat Immunol 9, 424-31 (2008).

32. Liou, J., Fivaz, M., Inoue, T. & Meyer, T. Live-cell imaging reveals sequential oligomerization and local plasma membrane targeting of stromal interaction molecule 1 after Ca2+ store depletion. Proc Natl Acad Sci U S A 104, 9301-6 (2007).

33. Barr, V. A. et al. Dynamic Movement of the Calcium Sensor STIM1 and the Calcium Channel Orai1 in Activated T Cells: Puncta and Distal Caps. Mol Biol Cell (2008).

34. Jayachandran, R. et al. Survival of mycobacteria in macrophages is mediated by coronin 1-dependent activation of calcineurin. Cell 130, 37-50 (2007).

35. Cai, L., Holoweckyj, N., Schaller, M. D. & Bear, J. E. Phosphorylation of coronin 1B by protein kinase C regulates interaction with Arp2/3 and cell motility. J Biol Chem 280, 31913-23 (2005).

36. Cai, L., Makhov, A. M. & Bear, J. E. F-actin binding is essential for coronin 1B function in vivo. J Cell Sci 120, 1779-90 (2007).

37. Appleton, B. A., Wu, P. & Wiesmann, C. The crystal structure of murine coronin-1: a regulator of actin cytoskeletal dynamics in lymphocytes. Structure 14, 87-96 (2006).

38. Cai, L., Marshall, T. W., Uetrecht, A. C., Schafer, D. A. & Bear, J. E. Coronin 1B coordinates Arp2/3 complex and cofilin activities at the leading edge. Cell 128, 915-29 (2007).

39. Niwa, R., Nagata-Ohashi, K., Takeichi, M., Mizuno, K. & Uemura, T. Control of actin reorganization by Slingshot, a family of phosphatases that dephosphorylate ADF/cofilin. Cell 108, 233-46 (2002).

40. Gomez, T. S. et al. HS1 functions as an essential actin-regulatory adaptor protein at the immune synapse. Immunity 24, 741-52 (2006).

41. Gomez, T. S. et al. Formins regulate the actin-related protein 2/3 complex-independent polarization of the centrosome to the immunological synapse. Immunity 26, 177-90 (2007).

42. Buckley, R. H. Molecular defects in human severe combined immunodeficiency and approaches to immune reconstitution. Annu Rev Immunol 22, 625-55 (2004).

43. McGhee, S. A., Stiehm, E. R. & McCabe, E. R. Potential costs and benefits of newborn screening for severe combined immunodeficiency. J Pediatr 147, 603-8 (2005).

44. Kovanen, P. E. & Leonard, W. J. Cytokines and immunodeficiency diseases: critical roles of the gamma(c)-dependent cytokines interleukins 2, 4, 7, 9, 15, and 21, and their signaling pathways. Immunol Rev 202, 67-83 (2004).

45. Check, E. Second cancer case halts gene-therapy trials. Nature 421, 305 (2003).

46. Reith, W. & Mach, B. The bare lymphocyte syndrome and the regulation of MHC expression. Annu Rev Immunol 19, 331-73 (2001).

47. Fischer, A., de Saint Basile, G. & Le Deist, F. CD3 deficiencies. Curr Opin Allergy Clin Immunol 5, 491-5 (2005).

48. Chan, A. C. et al. ZAP-70 deficiency in an autosomal recessive form of severe combined immunodeficiency. Science 264, 1599-601 (1994).

49. Elder, M. E. et al. Human severe combined immunodeficiency due to a defect in ZAP-70, a T cell tyrosine kinase. Science 264, 1596-9 (1994).

50. Goldman, F. D. et al. Defective expression of p56lck in an infant with severe combined immunodeficiency. J Clin Invest 102, 421-9 (1998).

51. Hubert, P. et al. Defective p56Lck activity in T cells from an adult patient with idiopathic CD4+ lymphocytopenia. Int Immunol 12, 449-57 (2000).

52. Kung, C. et al. Mutations in the tyrosine phosphatase CD45 gene in a child with severe combined immunodeficiency disease. Nat Med 6, 343-5 (2000).

53. Tchilian, E. Z. et al. A deletion in the gene encoding the CD45 antigen in a patient with SCID. J Immunol 166, 1308-13 (2001).

54. Macchi, P. et al. Mutations of Jak-3 gene in patients with autosomal severe combined immune deficiency (SCID). Nature 377, 65-8 (1995).

55. Russell, S. M. et al. Mutation of Jak3 in a patient with SCID: essential role of Jak3 in lymphoid development. Science 270, 797-800 (1995).

56. Puel, A., Ziegler, S. F., Buckley, R. H. & Leonard, W. J. Defective IL7R expression in T(-)B(+)NK(+) severe combined immunodeficiency. Nat Genet 20, 394-7 (1998).

57. Hardy, I., Gershon, A. A., Steinberg, S. P. & LaRussa, P. The incidence of zoster after immunization with live attenuated varicella vaccine. A study in children with leukemia. Varicella Vaccine Collaborative Study Group. N Engl J Med 325, 1545-50 (1991).

58. Ghaffar, F. et al. Disseminated infection with varicella-zoster virus vaccine strain presenting as hepatitis in a child with adenosine deaminase deficiency. Pediatr Infect Dis J 19, 764-6 (2000).

59. Kramer, J. M. et al. Disseminated vaccine strain varicella as the acquired immunodeficiency syndrome-defining illness in a previously undiagnosed child. Pediatrics 108, E39 (2001).

60. Kumar, R. A. et al. Recurrent 16p11.2 microdeletions in autism. Hum Mol Genet (2007).

61. Weiss, L. A. et al. Association between Microdeletion and Microduplication at 16p11.2 and Autism. N Engl J Med (2008).

62. Marshall, C. R. et al. Structural variation of chromosomes in autism spectrum disorder. Am J Hum Genet 82, 477-88 (2008).

63. Ghebranious, N., Giampietro, P. F., Wesbrook, F. P. & Rezkalla, S. H. A novel microdeletion at 16p11.2 harbors candidate genes for aortic valve development, seizure disorder, and mild mental retardation. Am J Med Genet A 143, 1462-71 (2007).

64. Ballif, B. C. et al. Discovery of a previously unrecognized microdeletion syndrome of 16p11.2-p12.2. Nat Genet 39, 1071-3 (2007).

65. Bourthoumieu, S. et al. First prenatally diagnosed case of 16p11.2p12.1 duplication. Prenat Diagn 28, 254-6 (2008).

Publishing Agreement

It is the policy of the University to encourage the distribution of all theses and dissertations. Copies of all UCSF theses and dissertations will be routed to the library via the Graduate Division. The library will make all theses and dissertations accessible to the public and will preserve these to the best of their abilities, in perpetuity.

Please sign the following statement:

I hereby grant permission to the Graduate Division of the University of California, San Francisco to release copies of my thesis or dissertation to the Campus Library to provide access and preservation, in whole or in part, in perpetuity.

Author Signature

6/12/08
Date